

NSWC/TR-79-351

12

A080315

BURNING TO DETONATION TRANSITION IN POROUS BEDS OF A HIGH ENERGY PROPELLANT

BY R. R. BERNECKER, D. PRICE
H. SANDUSKY

RESEARCH AND TECHNOLOGY DEPARTMENT

NOV 1979

Approved for public release, distribution unlimited.

DIG FILE COPY



NAVAL SURFACE WEAPONS CENTER

Dahlgren, Virginia 22448 • Silver Spring, Maryland 20910

452

UNCLASSIFIED

SECURITY CLASSIFICATION OF THIS PAGE (When Data Entered)

20. (Cont.) those observed for tetryl in previous studies. The effect of confinement on the DDT susceptibility of this material at high porosities is small.

UNCLASSIFIED

SECURITY CLASSIFICATION OF THIS PAGE (When Data Entered)

FOREWORD

The deflagration to detonation transition (DDT) behavior of porous charges of a high-energy propellant (VLU) has been studied at both high confinement (steel tube) and low confinement (plastic tube). The physical nature of the propellant used to construct the porous beds was varied: shredded, powdered and cuboid materials were evaluated. The major part of the accumulated data is for the shredded propellant.

In the high confinement apparatus it was demonstrated that pressurization along most of the predetonation column was mild. The region of accelerating pressure buildup, necessary for DDT, occurred shortly before (both in time and distance) a transition to detonation. This pressure buildup was associated with the propagation of compressive waves both forward and rearward in the predetonation period. The origin of the event producing these compressive waves is unknown but appears to be a rapid heat release mechanism (e.g., a thermal explosion) rather than a pressure buildup produced by confined (convective) burning. The DDT characteristics observed for this propellant are quite similar to those observed earlier for tetryl in the steel apparatus. The predetonation column lengths observed in the high and low confinement systems are comparable at high porosities. Thus, the effect of confinement on the DDT susceptibility of this material at high porosities is small although confinement would be expected to be more important at lower porosities.

This work was carried out under Task 80003-001/77402, Explosives Hazards Classification and HEPS. The present results and conclusion on the DDT behavior of VLU should be of interest in the area of propellant and explosive sensitivity as well as that of safety and reliability of weapons.

The text of this report was presented as a paper at the 16th JANNAF Combustion Meeting, Monterey, California, 10 September 1979.

Julius W. Enig
JULIUS W. ENIG
By direction

CONTENTS

	<u>Page</u>
INTRODUCTION.	1
EXPERIMENTAL ARRANGEMENTS AND PROCEDURES.	2
EXPERIMENTAL RESULTS AND DISCUSSION.	5
Steel DDT Tube.	5
Lexan DDT Tube.	16
SUMMARY AND CONCLUSIONS OF DDT EXPERIMENTS WITH VLU PROPELLANT.	29
REFERENCES.	31
APPENDIX A ADDITIONAL DATA.	A-1

TABLES

<u>Table</u>	<u>Page</u>
1 Summary of DDT Characteristics for VLU Propellant in Steel Tube.	13
2 Summary of Predetonation Fronts for Shredded VLU Propellant in Lexan Tube.	22
3 Summary of DDT Experiments with Shredded Porous Propellant.	29
A1 Detailed Data for Shredded VLU-10.	A-6
A2 Detailed Data for Powdered VLU-10.	A-9
A3 Detailed Data for Cubes and Slugs of VLU-10.	A-11

ILLUSTRATIONS

<u>Figure</u>		<u>Page</u>
1	Cross Section of Lexan Tube.	3
2	Experimental Arrangement for Transparent (Lexan) EDT Tube.	4
3	Photomicrographs of VLU Samples.	6
4	Distance-Time Data for Shot 709 with Shredded VLU at 54.3% TMD, $\rho_0 = 1.02 \text{ g/cm}^3$	7
5	Data for Shot 1217 with Granular VLU at 53.7% TMD, $\rho_0 = 1.01 \text{ g/cm}^3$	9
6	Data for Shot 804 with Shredded VLU at 70.7% TMD, $\rho_0 = 1.33 \text{ g/cm}^3$	10
7	Data for Shot 803 with Shredded VLU at 78.7% TMD, $\rho_0 = 1.48 \text{ g/cm}^3$	12
8	Dependence of Predetonation Column Length on Initial Compaction.	15
9	Relative Times to Detonation as Functions of %TMD.	17
10	Relations between Predetonation Column Length and Relative Times to Detonation.	18
11	Selected Camera Frames from Shot S44 with Shredded VLU at 58.5% TMD, $\rho_0 = 1.10 \text{ g/cm}^3$	20
12	Data for Shot S-44 with Shredded VLU at 58.5% TMD, $\rho_0 = 1.10 \text{ g/cm}^3$	21
13	Selected Camera Frames from Shot S45 with Shredded VLU at 58.5% TMD, $\rho_0 = 1.10 \text{ g/cm}^3$	24
14	Data for Shot S45 with Shredded VLU at 58.5% TMD, $\rho_0 = 1.10 \text{ g/cm}^3$	26
15	Selected Camera Frames from Shot S46 with Shredded VLU at 63.8% TMD, $\rho_0 = 1.2 \text{ g/cm}^3$	27
16	Data for Shot S46 with Shredded VLU at 63.8% TMD, $\rho_0 = 1.20 \text{ g/cm}^3$	28

ILLUSTRATIONS

<u>Figure</u>	LIST OF ILLUSTRATIONS FOR APPENDIX	<u>Page</u>
A1	Shot 1001 on 90.5% TMD sVLU-10, $\rho_0 = 1.70 \text{ g/cm}^3$	A-12
A2	Shot 902 on 86.6% TMD sVLU-10, $\rho_0 = 1.63 \text{ g/cm}^3$	A-13
A3	Shot 802 on 82.6% TMD sVLU-10, $\rho_0 = 1.55 \text{ g/cm}^3$	A-14
A4	Shot 803 on 78.7% TMD sVLU-10, $\rho_0 = 1.48 \text{ g/cm}^3$	A-15
A5	Shot 817 on 74.5% TMD sVLU-10, $\rho_0 = 1.40 \text{ g/cm}^3$	A-16
A6	Shot 712 on 74.5% TMD sVLU-10, $\rho_0 = 1.40 \text{ g/cm}^3$	A-17
A7	Shot 710 on 64.4% TMD sVLU-10, $\rho_0 = 1.21 \text{ g/cm}^3$	A-18
A8	Shot 901 on 60.4% TMD sVLU-10, $\rho_0 = 1.14 \text{ g/cm}^3$	A-19
A9	Shot 709 on 54.3% TMD sVLU-10, $\rho_0 = 1.02 \text{ g/cm}^3$	A-20
A10	Shot 1219 on 86.2% TMD pVLU-10, $\rho_0 = 1.62 \text{ g/cm}^3$	A-21
A11	Shot 1201 on 83.8% TMD pVLU-10, $\rho_0 = 1.58 \text{ g/cm}^3$	A-22
A12	Shot 1016 on 74.6% TMD pVLU-10, $\rho_0 = 1.40 \text{ g/cm}^3$	A-23
A13	Shot 1211 on 65.4% TMD pVLU-10, $\rho_0 = 1.23 \text{ g/cm}^3$	A-24
A14	Shot 1104 on 69.6% TMD cubed VLU-10, $\rho_0 = 1.12 \text{ g/cm}^3$	A-25
A15	Shot 711 on 58.5% TMD cubed VLU-10, $\rho_0 = 1.10 \text{ g/cm}^3$	A-26
A16	Shot 808 on ~100% TMD slugs of VLU-10 $\rho_0 \sim 1.88 \text{ g/cm}^3$	A-27
A17	Detonation Velocity of VLU-10 as a Function of %TMD.	A-28

INTRODUCTION

The mechanism of the deflagration to detonation transition (DDT) has been discussed in some detail in recent years.^{1,2a} However, there have been few systematic studies of the DDT process as it applies to porous beds of propellants. Korotkov et al. have looked at mixtures of ammonium perchlorate (AP) with polystyrene or with TNT.^{1,3} For these composite mixtures, a different dependence of predetonation column length (ℓ) on density was observed. There was an apparent continuous increase in ℓ for increasing density, over the compaction range of 40 to 75% theoretical maximum density (TMD). This contrasts with the U-shaped ℓ -%TMD curves found for neat explosives.^{1,4}

Shuey and coworkers^{5,6} conducted some of the earliest investigations into the susceptibility of various double base propellants to DDT. They demonstrated not only that these materials could transit to detonation from a burning mode but that the transition would occur under relatively low confinement. More recently, Beckstead and coworkers have shown that porous beds of various (obsolete) friable, cross-linked double-base (XLDB) propellants could also undergo DDT under low confinement.^{7,8} They have systematically varied the permeability of the porous bed (as reflected in the porosity and particle surface to volume ratio for burning) in determining the propensity to transit to detonation.

The present work was undertaken to assess the susceptibility of a XLDB propellant to transition to detonation under conditions of both high and low confinement. In particular it was of interest to contrast the mechanistic aspects of this propellant with those observed for various explosives. Consequently the thickwalled steel tube arrangement used in earlier explosive studies^{2b} has been employed here to study DDT under high confinement. For conditions of low confinement, a recently developed transparent plastic DDT tube arrangement has been used.⁹ The latter system is useful in extending our knowledge of the early DDT events. The propellant used herein was the friable (obsolete) formulation, VLU. The physical nature of the propellant used to construct the porous beds was varied: powdered and shredded material, as well as cubes of propellant, were evaluated. The major part of the accumulated data is for shredded material.

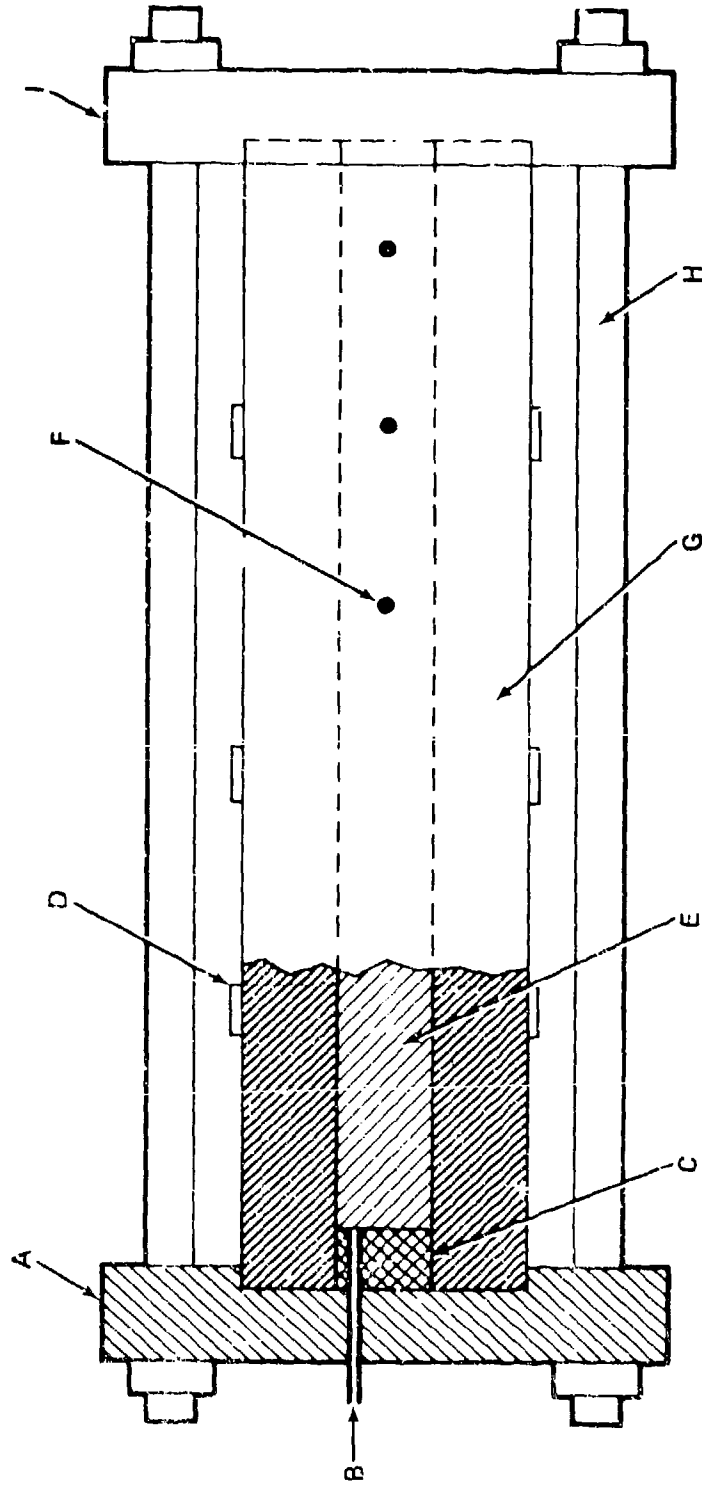
EXPERIMENTAL ARRANGEMENTS AND PROCEDURES

The thickwalled steel tube arrangement and procedures have been described in detail elsewhere.^{2,4} It consists of a seamless steel tube with heavy end closures. The column length of the 0.35 g of 25/75 B/ KNO_3 ignitor is 6.4 mm; the length of the explosive column is 295.4 mm. The tube is instrumented with ionization probes (IPs) and strain gages (SGs) to monitor ionization fronts and internal pressure, respectively. Both custom-made and commercial IPs are used and data from each type of probe are distinguished on later graphs. The strain gage output is reported in microstrain ($\mu\epsilon$). In a static calibration of the tube, the gradient is 1120 $\mu\epsilon/\text{GPa}$ (1.135 $\mu\epsilon/\text{atm}$) up to the elastic limit of 0.226 GPa (2192 atm). From 0.22 to 0.47 GPa the strain level increases from 246 $\mu\epsilon$ to 788 $\mu\epsilon$.

The transparent plastic tube arrangement is described in detail in Reference 9. A schematic representation of the instrumental tube is shown in Figure 1 and the experimental arrangement is shown in Figure 2. The tube is machined from polycarbonate rod; the commercial designation of the polycarbonate plastic is Lexan 101-111. Although Lexan 101-111 has good transmittance of light, it was found in this work that better transmittance could be attained through the machined tube by "solvent polishing" with ethylene dichloride. Both the inner diameter (ID) and outer diameter (OD) of the Lexan tube are greater than the ID and OD of the steel tube. The length of the propellant bed varied from 253.4 to 289.6 mm in this work. As shown in Figure 1, the Lexan tube, loaded in the same manner as the steel DDT tube, is clamped between two 25 mm thick steel plates using four threaded (19 mm diameter) steel rods. The ignitor utilizes a column length of B/ KNO_3 identical to that for the steel tube but has a scaled diameter such that the ratio of the cross-sectional area of the B/ KNO_3 to the cross-sectional area of the propellant is the same for both the Lexan and steel tube. Here the weight of B/ KNO_3 used is about 0.75 g.

The instrumentation used with the Lexan tube includes the ionization probes and strain gages used with the steel tube. However, in some instances the commercial ionization probes are attached to electrical circuits which continuously monitor resistance across the head of the probe. When used in this manner, the commercial probe is called a conductivity probe. (A single conductivity probe was occasionally used in the steel DDT tube experiments.) A major difference in the SG data between the steel DDT tube and the Lexan tube is the strain and pressure gradient. For the Lexan tube, a static calibration has at present been made only to 11.1 MPa (110 atm). The experimental results agree within 7% with the calculated $d\epsilon/dp$ values. The latter values show a gradient of 108 $\mu\epsilon/\text{MPa}$ (10.9 $\mu\epsilon/\text{atm}$) up to 28 MPa (276 atm), the estimated elastic limit of the Lexan tube.

An optical fiber/photocell (OF/PC) assembly is used to detect luminosity along the ignitor/propellant interface. The optical fiber is threaded through orifices in the ignitor plate and a steel sleeve around the ignitor. The output of the OF/PC assembly is used to trigger recording oscilloscopes and an electronic flash; the latter is used to



A - STEEL IGNITOR PLATE; B - OPTICAL FIBER; C - IGNITOR SECTION;
 D - STRAIN GAGE; E - PROPELLANT COLUMN; F - CONDUCTIVITY PROBE LOCATION;
 G - LEXAN TUBE; H - STEEL CONNECTING BOLT; I - STEEL CLOSURE PLATE.
 INNER DIAMETER = 25.4 mm, OUTER DIAMETER = 76.2 mm

FIGURE 1 CROSS SECTION OF LEXAN DDT TUBE

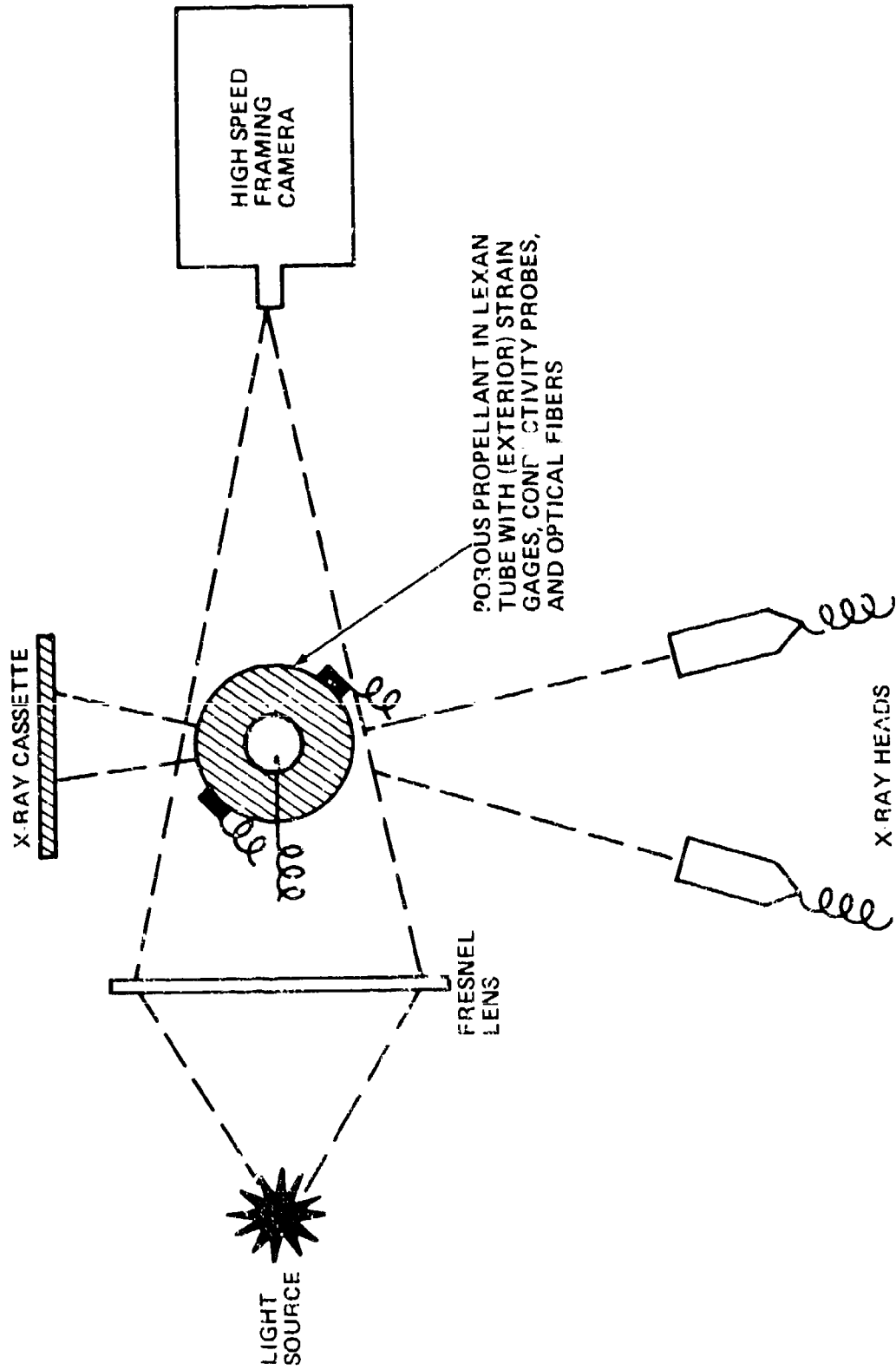


FIGURE 2 EXPERIMENTAL ARRANGEMENT FOR TRANSPARENT (LEXAN) DDT TUBE

backlight the Lexan tube for photographic coverage. The first appearance of backlighting on the camera's film serves as a temporal fiducial for the camera records and data from the oscilloscopes. In the Lexan DDT experiments zero time is the time of detection of luminosity by the OF/PC assembly.

To record the luminous events occurring in the Lexan system, a Beckman-Whitley Dynafax framing camera, Model 326, was used. This is a continuous access, rotating drum camera which records 224 frames (16 mm size) at a maximum rate of 25,000 fps. A more recent addition to the Lexan tube arrangement shown in Figure 2 is a flash radiography unit: Field Emission Corp., Model 235. The 150 kilovolt pulsers have a pulse width of 0.1 μ sec. Currently two x-ray heads can be pulsed during a DDT experiment. In the present work, flash radio-graphic data were not successfully obtained because the x-ray film and cassette were badly damaged. A new cassette arrangement has been developed and successfully utilized in subsequent work. To record the times associated with the various events (i.e., first detection of luminosity at ignitor interface, x-ray, etc), an electronic unit is used to record and display the order of a sequence of eight events and measure the time interval between them.

The propellant materials (shreds, granular powders, and cuboids) used to fabricate the porous charges were made by shredding, slicing or tearing solid pieces of VLU. The resultant shredded and granular (powder) particles showed rough surfaces and irregular shapes. The cubes were more regular and the 1/16 in. cubes did have an average edge dimension of 1.6 mm; the 1/8 in. cubes were less regular. Photomicrographs of the granular powder indicated particle sizes ranging from 100 μ m to 1200 μ m. The shreds typically had "rectangular" dimensions of 0.5 mm by 1.6 mm by 25 mm. Fig. 3 shows photomicrographs of the powdered (p), shredded (s) and cubed VLU-10.

EXPERIMENTAL RESULTS AND DISCUSSION

STEEL DDT TUBE

This experimental investigation was directed primarily toward evaluating various predetonation parameters as the porosity of the propellant beds was systematically varied. The majority of the accumulated data in steel DDT tubes pertain to the shredded material; ten experiments were run with this material over the density range of 1.0 to 1.7 g/cc (54 to 91% theoretical maximum density, TMD). Five experiments were run with the granular powder over the range of 1.0 to 1.6 g/cc (54 to 86% TMD) while only two shots were fired with the cuboid material at 60% TMD.

Early in the study it was observed at the lower densities that ionization probes, used to trigger our recording instrumentation and to outline the propagation of predetonation fronts, did not respond in the earlier (nearer the ignitor) portion of the predetonation column. Moreover the response of the IPs appeared to depend upon the initial physical stage of the propellant material. Figure 4 and 5a show this feature for shredded and granular charges at 54% TMD. In Figure 4 (Shot 709), IPs did not respond until just before a transition to detonation (the location of the onset

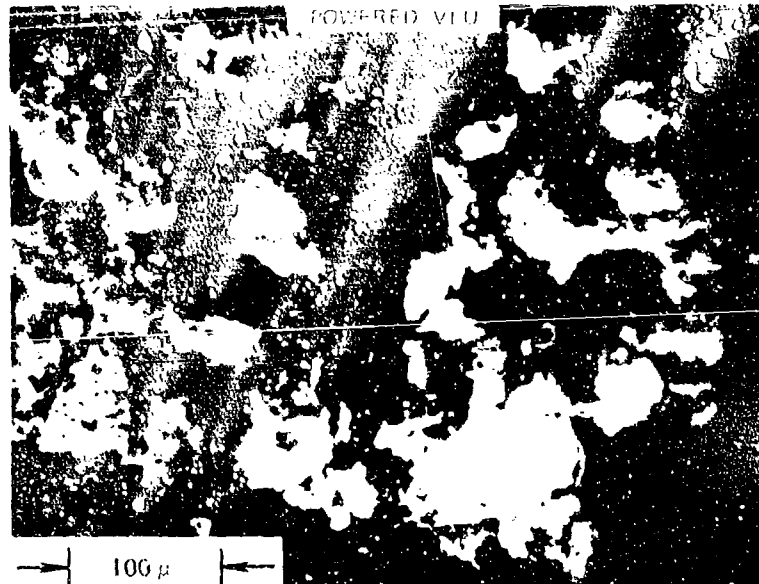
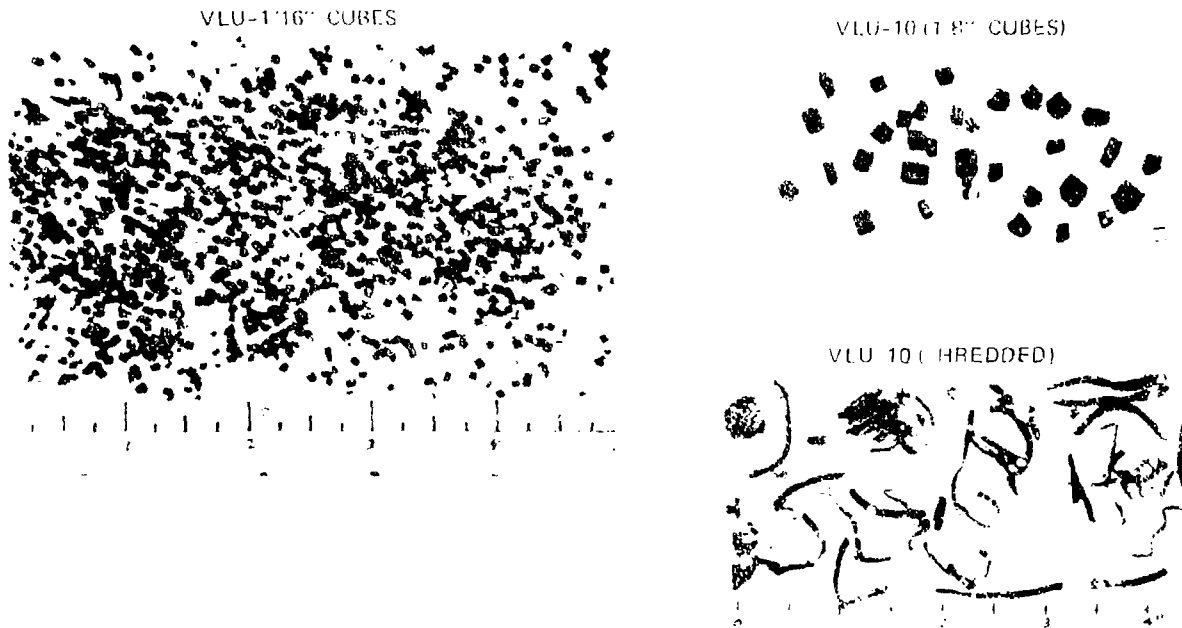


FIGURE 3 PHOTOMICROGRAPHS OF VLU SAMPLES

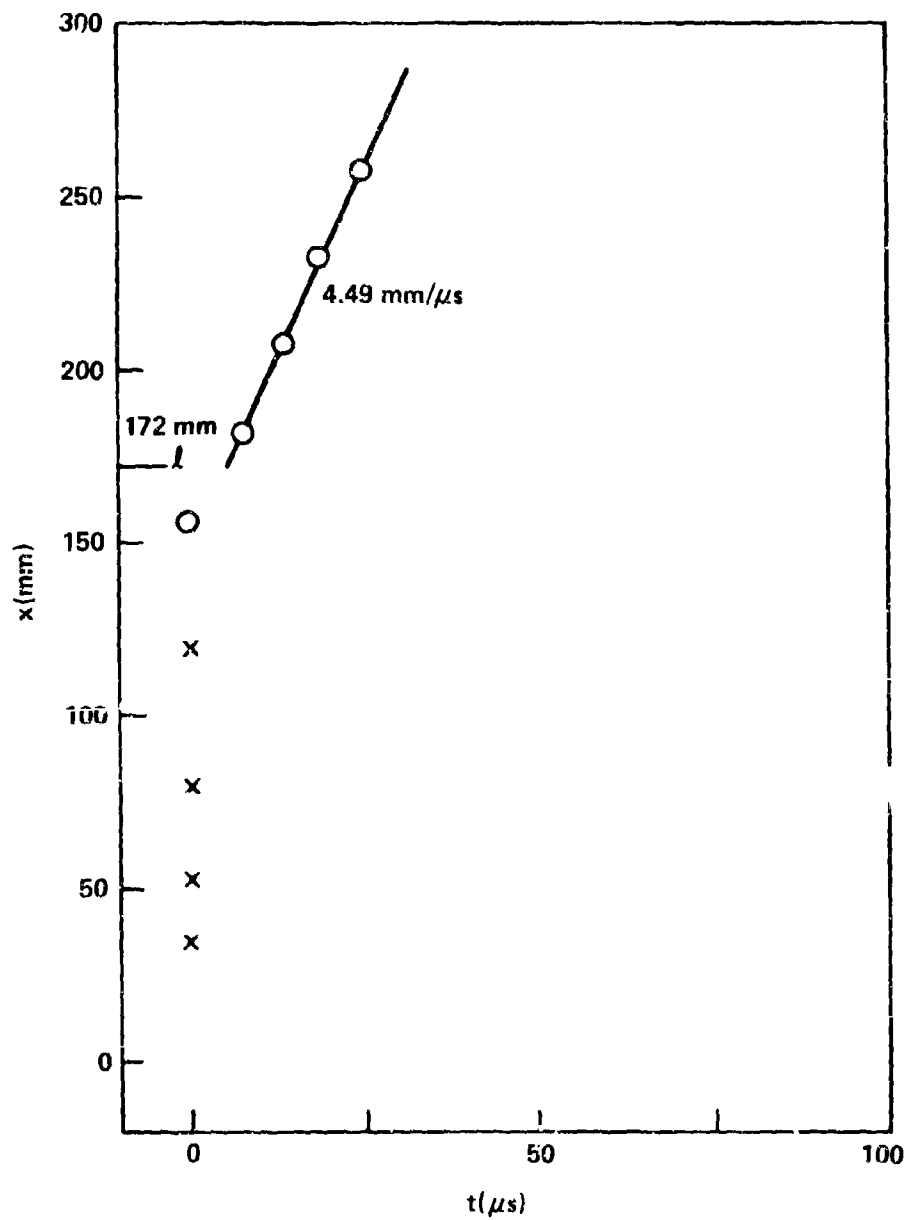


FIGURE 4 DISTANCE-TIME DATA FOR SHCT 709 WITH SHREDDED VLU AT 54.3% TMD, $\rho_o = 1.02 \text{ g/cc}$. (○ RESPONSE OF NSWC PROBE, x LOCATION OF NSWC PROBE - NO RESPONSE)

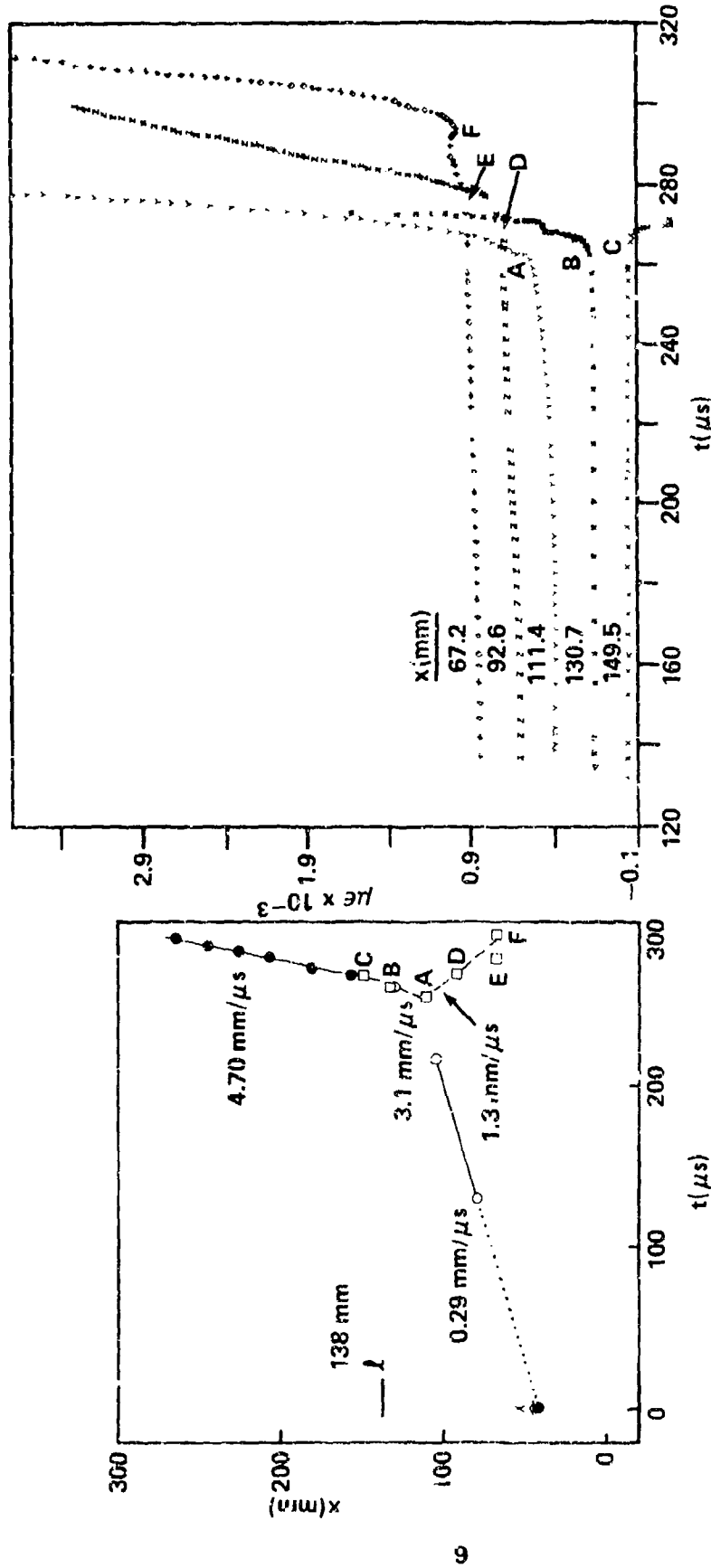
of detonation is 172 mm and is deduced primarily from markings on the recovered tube fragments). Custom-made IPs located at 34, 54, 80 and 118 mm did not respond either before or after the transition to detonation (here x is 138 mm). In Shot 1217 a conductivity probe* was used at the 42 mm location; it responded 129.5 μ s before any of our regular (custom-made or commercial) probes. The response time of this 42 mm probe serves as zero time in Figure 5. It is interesting to note that a custom-made IP at 54 mm failed to respond but similar probes at 80 mm and 105 mm did respond. The responses of the 42, 80 and 105 mm probes appear to outline the propagation of a convective ignition front, travelling at 0.29 mm/ μ s.

The failure of our regular probes to trigger early in the predetonation period potentially limits information concerning pressure buildup, obtained from our SG data. Fortunately it was found that pressurization during the predetonation period was unusually mild over a large portion of the predetonation column. This feature is illustrated in the SG data of Figure 5b for the 54% TMD granular material. From these data it was found that at 253 μ s (10 μ s before the onset of detonation) the maximum pressure observed at any of the SG locations was about 100 MPa (1000 atm). Thereafter, pressure (strain) began to increase rapidly, first at the 111 mm location and subsequently at all other SG locations in the predetonation region. The time at which the rapid pressurization began is represented by a square (\square) symbol in the x-t plot of Figure 5a, letters, associated with this symbol, show corresponding data in Figures 5a and 5b**. In Figure 5a points A and B outline the propagation of a forward traveling compressive wave whose velocity is about 3.1 mm/ μ s while points A, D, and F outline a rearward travelling compressive wave whose velocity is about 1.3 mm/ μ s. (Point E is associated with a rearward compressive wave traveling through the steel wall; this phenomena is discussed in more detail below.) These data lead to the conclusion that the region in which accelerating pressure buildup is first detected is relatively near to the location of onset of detonation.

Similar conclusions concerning the origin of pressure buildup in charges using shredded VLU can be drawn from the data in Figures 6 and 7. Figure 6 presents the data for shredded VLU pressed to 70.5% TMD while Figure 7 pertains to a 78.6% TMD charge. In Figure 6a, the response of IPs at 92 and 118 mm indicate that a convective ignition front is propagating downstream at a velocity of 0.34 mm/ μ s. Probes at 41 and 67 mm did not respond, during the experimental time period, to this convective front or any other process. The SG data of Figure 6b show that accelerating pressure buildup within the porous charge does not begin until 140 μ s or 12 μ s before a transition to detonation occurred. As seen in the predetonation period of Figure 6a, points A and C define a rearward compressive wave traveling at 1.55 mm/ μ s. Point B is associated with a forward traveling compressive wave (dashed line); the response of the 158 mm IP appears to be associated with reaction induced by forward traveling compressive waves. The origin of the event leading to the propagation of these compressive waves appears to be located slightly beyond 140 mm or less than 30 mm from the onset of detonation.

*A conductivity probe is a special IP and is described in the Experimental Arrangements and Procedures section.

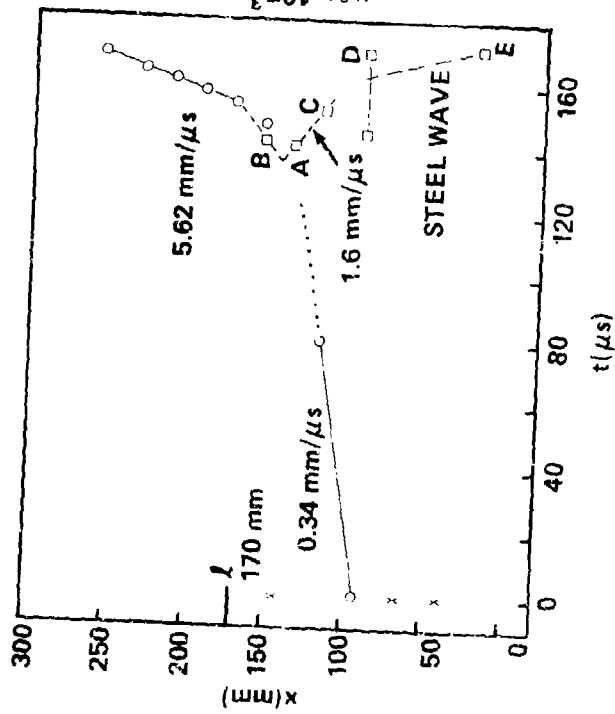
**The data from the 149.5 mm location show a typical ϵ -t curve when the SG is located in the detonation region or close to the onset of detonation.



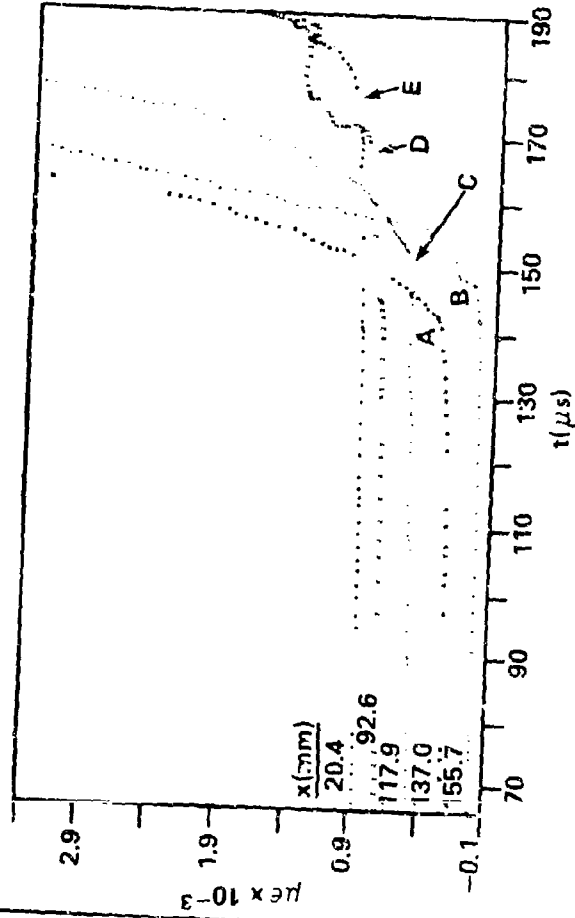
a. DISTANCE-TIME PLOT (O RESPONSE OF NSWC PROBES ● RESPONSE OF COMMERCIAL PROBE, ● RESPONSE OF CONDUCTIVITY PROBE X LOCATION OF NSWC PROBE-NO RESPONSE, □ CHANGE IN SLOPE FROM $\epsilon-t$ CURVE OF b)

b. STRAIN-TIME PLOTS (CHANGE OF SLOPE SHOWN BY LETTERS WHICH ALSO APPEAR IN a. EACH CURVE EXCEPT THE LOWEST HAS BEEN RAISED $0.2 \times 10^{-3} \mu\epsilon$, OR AN INTEGRAL MULTIPLE THEREOF, FOR BETTER DATA DISPLAY.)

FIGURE 5 DATA FOR SHOT 1217 WITH GRANULAR VLU AT 53.7% TMD, $\rho_0 = 1.01 \text{ g/cm}^3$



a. DISTANCE-TIME PLOT (KEY OF FIGURE 5a)



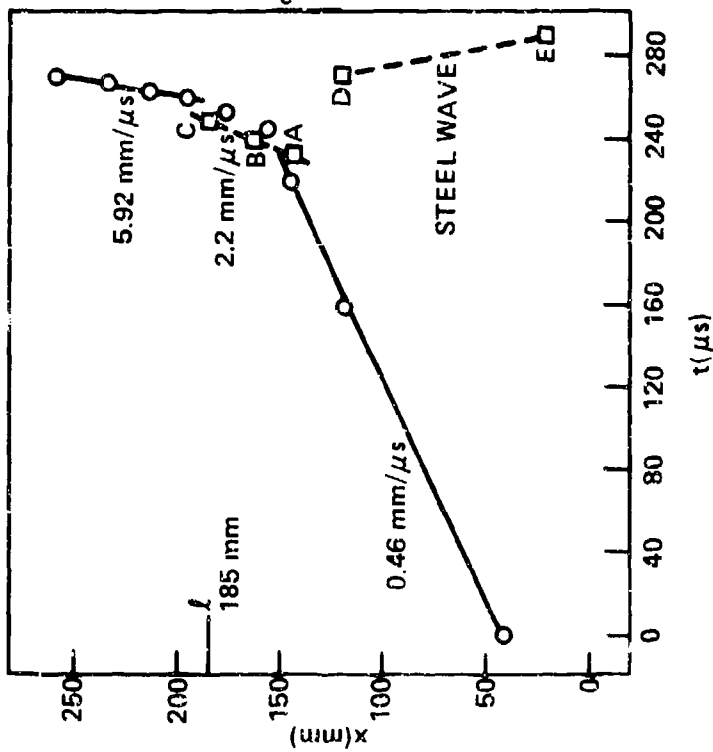
b. STRAIN-TIME PLOTS (KEY OF FIGURE 5b)

FIGURE 6 DATA FOR SHOT 804 WITH SHREDDED VLU AT 70.7% TMD, $\rho_0 = 1.33 \text{ g/cc}$

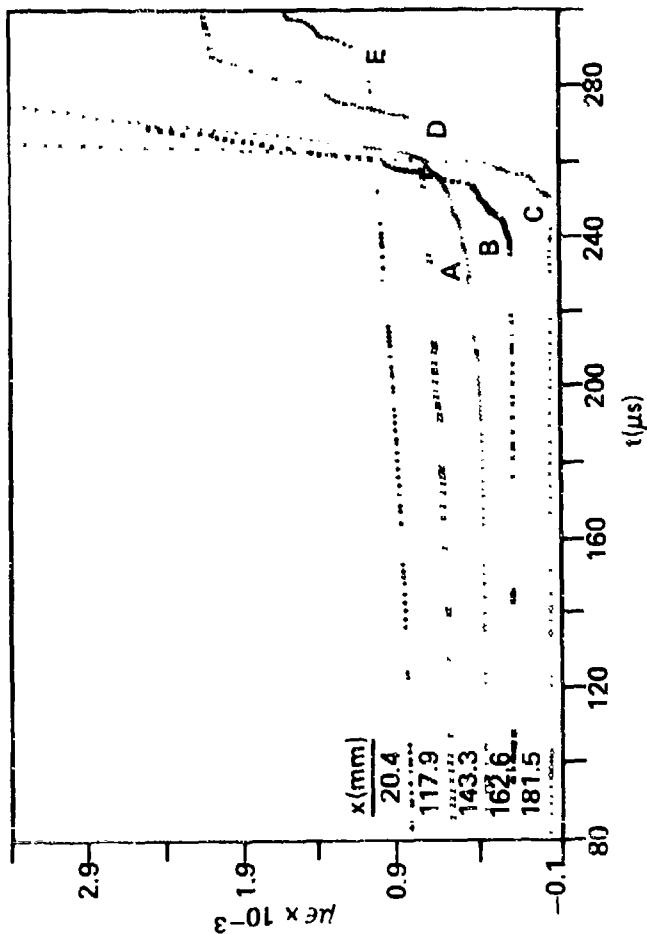
In Figure 7 the IP and SG data from the 78.6% TMD shredded VLU charge confirm the previous interpretation and serve to illustrate more clearly the propagation path of the forward traveling compressive wave. In this experiment the response of the first few IPs was associated again with a convective ignition front whose velocity was about 0.46 mm/ μ s. Strain gage data (taken from Figure 7b) for the 143, 163, and 182 mm locations outline a forward traveling compressive wave (points A, B, and C) whose velocity is about 2.2 mm/ μ s. The interpretation of the path of the rearward traveling wave is somewhat unclear. Points D and E appear to be associated with a wave traveling at a velocity of about 5.7 mm/ μ s and having its origin close to the onset of detonation. From the gradients associated with increase in strain beyond points D and E in the SG data of Figure 7b and the 5.7 mm/ μ s velocity of this wave, it is concluded that this rearward traveling wave is a compressive wave traveling through the steel wall and not through the propellant bed. This steel compressive wave, as it shall be called, has also been observed in several other experiments with VLU (see Appendix A) and earlier work with explosives;¹⁰ in these cases at least three SG locations were used to define its propagation path and associated $d\epsilon/dt$ values.

Table 1 summarizes the various experimental parameters associated with the DDT mechanism in porous charges of VLU. The first reaction front which we have detected with our IPs and SGs in the majority of the experiments seemed to be a convective ignition front (CIF). In a few experiments (Shots 802, 817, and 1201) this front had a lower velocity (~ 0.12 mm/ μ s) close to the ignition region but later attained a velocity consistent with CIF velocities in experiments at slightly higher densities. In view of the difficulty in response experienced with the IPs in porous beds of VLU, this observation of two distinct velocities could be attributed to experimental variabilities. However, as described below for the Lexan experiments, this same type of behavior is also observed for a luminous CIF. Hence it is concluded that the variability of CIF velocity in a given experiment is a manifestation of the permeability and turbulent flow within the porous bed. On the whole, the data for the CIF in Table 1 show little dependence on porosity and permeability; the average value for all experiments is about 0.3 mm/ μ s.

In the predetonation period, compressive waves have been observed to originate close to the onset of detonation and travel in both forward and rearward directions. The detection of the forward compressive wave has been most difficult because at least two SG locations (needed to outline its path) must be precisely located in a region a few centimeters before the onset of detonation. Consequently data concerning the velocity of the forward traveling compressive wave have been obtained for only three experiments although many other experiments show the response of one SG which is consistent with the presence of this wave. However, there can be no doubt about the existence of a forward traveling compressive wave since its presence is required for the final stage in the DDT mechanism, the shock-to-detonation (SDT) stage.



a. DISTANCE-TIME PLOT (KEY OF FIGURE 5a)



b. STRAIN-TIME PLOT (KEY OF FIGURE 5b)

FIGURE / DATA FOR SHOT 803 WITH SHREDDED VLU AT 78.7% TMD, $\rho_o = 1.48$ g/cc

TABLE 1 Summary of DDT Characteristics for VLU Propellant in Steel Tube

Shot No. SHREDED	ρ ₀ g/cc	% TMDa	Front Velocity, mm/μs				Predet. Column Length mm	Relative times to Detonation, μs	
			Convective	Compressive Forw'd	Rearw'd	Detonation		41 Δt _D	156 Δt _D
1001	1.70	90.4	0.31	-	3.9	6.58(0.16) ^c	360	-	231
902	1.63	86.7	~0.4	~1.5	2.6	7.19(0.11)	232	(347) ^e	73
802	1.55	82.4	0.13-0.25	-	-	6.05(-)	206	(590)	30
803	1.48	78.7	0.46	2.2	-	5.92(0.50)	185	(269)	25
817	1.40	74.5	0.12-0.3	-	-	-	F	-	-
712	1.40	74.5	0.22	-	~1.5	6.08(0.39)	149	-	-
804	1.33	70.7	0.34	-	1.6	5.62(0.14)	170	-	5.4
710	1.21	64.4	~0.3	-	?	5.39(0.39)	194	-	(100)
901	1.14	60.6	b	-	?	5.05(0.09)	168	-	5.3
709	1.02	54.3	b	-	1.7	4.49(0.14)	172	-	6.0
POWDER									
1219	1.62	86.2	b	-	-	6.94(0.45)	222	-	45
1201	1.58	84.0	0.12-0.5	-	1.6	6.17(0.42)	214	440	37
1016	1.40	74.5	0.20	-	1.6	6.22(0.18)	166	372**	6
1211	1.23	65.4	0.21	-	2.0	5.55(0.18)	134	228	-
1217	1.01	53.7	0.29	3.1	1.3	4.70(0.07)	138	263	-
CUBES*									
1104	1.12	59.6	b	-	-	4.97(-)	232	-	(73.5)

a. Voidless density is 1.89 g/cc. b. Insufficient data base. c. Standard deviation.
d. Times are relative to discharge of IP at x = 41 mm or at x = 156 mm as indicated by leading
superscript. e. Values in parentheses from records with erratic IP response.
* Nominally 1/16-in. cubes; 1/4-in. cubes failed to exhibit DDT in this experiment.
** Extrapolated.

The rearward traveling compressive wave seen in the predetonation period has been established in experiments covering a wide density range, 1.0 to 1.7 g/cc. The measurement of its velocity has been complicated, however, by the presence of another rearward traveling compressive wave, the "steel wave". The latter appears to be associated with the excitation within the steel wall of a compressive wave as a result of the onset of detonation. Nevertheless, in nine experiments it has been possible (as seen in Table 1) to assign a velocity to the predetonation rearward traveling wave; there appears to be a weak dependence on porosity. The velocity of this rearward wave should depend upon the density of (or along) the predetonation column. Since extensive compaction can occur (and has been established as occurring¹¹) in porous propellant beds, during the predetonation period, the velocity of the rearward traveling wave will be a manifestation of the extent of prior compaction and the extent of prior reaction.

The presence of the forward and rearward traveling compressive waves in the predetonation period as well as the location of the region of initial accelerating pressure along the predetonation column provide valuable information concerning the DDT mechanism in porous charges of VLU. These facts are indicative of a rapid heat release mechanism (e.g., a thermal explosion) as the driving force for a transition to detonation rather than a pressure buildup produced by confined (convective) burning. This sequence of events is not unique to DDT behavior in porous reactive beds; similar observations have been made for porous tetryl charges.¹²

Another similarity between the experimental data for porous VLU charges and tetryl charges is the dependence of the predetonation column length λ on % TMD. In Figure 8 are displayed the data from all VLU charges. For the shredded VLU beds, λ seems to be constant (within experimental error) below 75% TMD. As the compaction increases above 75% TMD, λ increases very sharply and indeed DDT could only be attained at 90% TMD by joining two of our regular DDT tubes to make a very long porous column. Although fewer experiments were conducted with the granular VLU material, the dependence of λ on % TMD for the granular material appears to be similar to the shredded material with one exception. At low compactions (< 70% TMD), the predetonation column length for granular material is less than values for the shredded material. If it is assumed that the permeability of a shredded charge is less than that of a granular charge at densities of 1.1 g/cc or less, the predetonation column length data from the shredded and granular materials can be interpreted as indicating that the more permeable charges have a shorter λ value. This also was the trend observed for porous tetryl charges. The data in Figure 8 from the shredded (and possibly the granular) VLU charges indicate that if there is a minimum in the λ -% TMD curve it is very shallow; this too was the case for (granular) 20 μ m tetryl¹² and the granular 15 μ m AP mixtures studied by Korotkov et al.³ Consequently at high confinement, porous charges of VLU exhibit many similarities in DDT behavior to porous charges of tetryl and somewhat similar behavior to some AP mixtures.

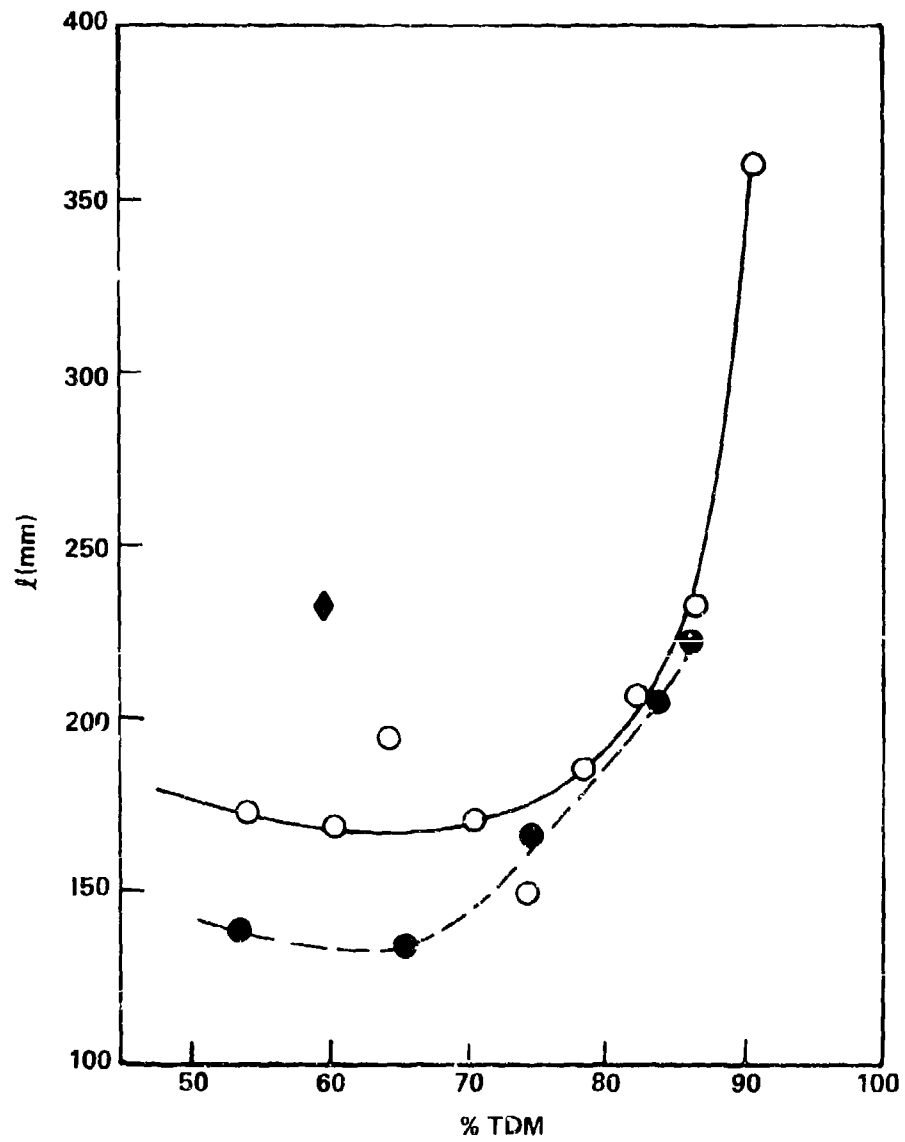


FIGURE 8 DEPENDENCE OF PREDETONATION COLUMN LENGTH ON INITIAL COMPACTION
(O SHREDDED VLU, ● POWDERED VLU, ◆ CUBOID VLU)

In the case of tetryl, erratic response of the earlier IPs resulted in values of Δt_D (relative time to detonation with respect to a specified x value) from which no smooth trend was evident. Here we have measured relative time with respect to IPs at 41 and 156 mm, respectively. The values are given in Table 1 and plotted vs % TMD in Fig. 9. Except for one value, the $156\Delta t_D$ vs % TMD values for shredded and ground VLU fall on smooth curves (Fig. 9a) drawn as were those of Fig. 8 with a shallow minimum at about 65% TMD. The two curves are within experimental error in Δt_D . The one point off the curve is from a shot in which early IP response was erratic. The values in parentheses in the Δt_D columns of Table 1 were read from similar records, and have been omitted from the plot of Fig. 9b. This latter "curve" of $41\Delta t_D$ vs % TMD is sketched by only four sets of data, one of which is extrapolated, because IPs at $x \sim 41$ mm often failed to respond in VLU; when they did, the records were apt to indicate erratic front behavior. This last was the case for the three shredded VLU charges which exhibited early response. However, the granulated material produced good IP records (see Appendix A) from which the data of Fig. 9b were obtained. Those data indicate a significant, though still shallow, minimum in $41\Delta t_D$ at about 65% TMD.

The trend Δt_D vs % TMD of Fig. 9 is very like that roughed out by the coarse tetryl data. It is the opposite of that observed for waxed RDX^{2,13}, picric acid,⁴ and PETN¹⁴ which exhibit decreasing Δt_D with increasing % TMD. Moreover, as the similarity of the curves of Figs. 8 and 9 suggest, there is a regular variation of λ with Δt_D as Fig. 10 shows. This too differs from the behavior of waxed RDX et al. where no analogous smooth curve, λ vs Δt_D , is evident for constant composition with varied compaction.

Since VLU clearly does not start its accelerated burning in the region near the ignitor, it does not generate a compressive wave from that region, marking the start of such a process. Such a wave, called the post-convective wave, provides data to compute another relative detonation time for most explosives. Obviously, it is non-existent for VLU.

LEXAN DDT TUBE

Only three experiments have been run with the shredded VLU propellant in the experimental arrangement shown in Figure 3; of these, one failed to transit to detonation. As mentioned earlier, no flash radiographic data were obtained because of system malfunction and/or inadequate protection of the x-ray film. However, use of SGs in conjunction with the framing camera has allowed us to extend our knowledge of the early stages of the DDT process.

Two experiments were run with shredded VLU at 1.10 g/cc (58.5 % TMD). Our philosophy has been to evaluate the confinement provided by the Lexan tube in the absence of any probe holes (e.g., for conductivity probes) which

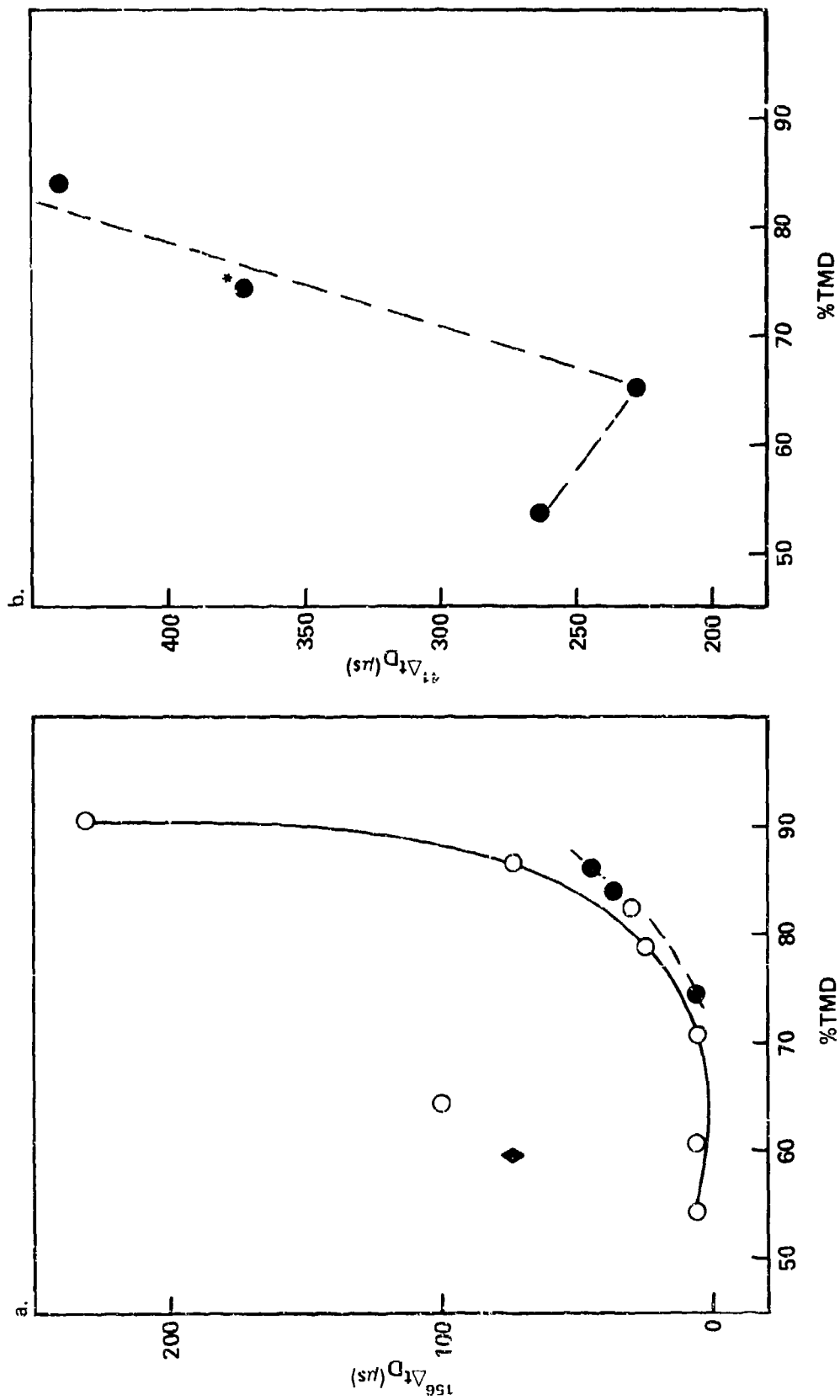


FIGURE 9 RELATIVE TIMES TO DETONATION AS FUNCTIONS OF %TMD (KEY OF FIGURE 8; *EXTRAPOLATED)

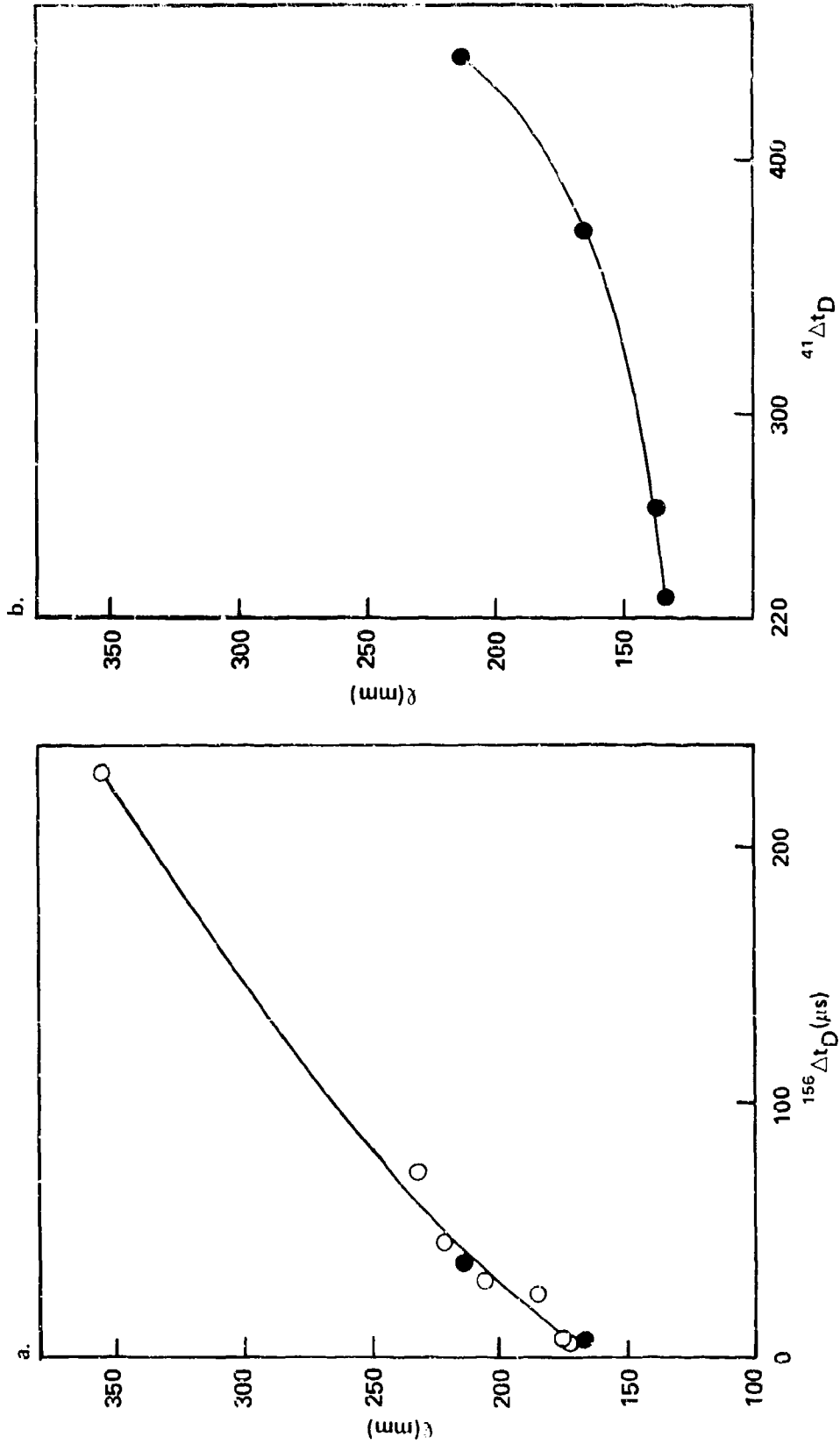


FIGURE 10 RELATIONS BETWEEN PREDETONATION COLUMN LENGTH AND RELATIVE TIMES TO DETONATION. (KEY OF FIGURE 9)

tend to reduce the effective confinement of the charge. Thus, in the first VLU experiment at 58.5% TMD (Shot S44), no conductivity probes were used although SGs were located along the length of the 253.4 mm porous column. An optical fiber/photocell (OF/PC) assembly was used to detect the luminosity at the ignitor/propellant interface ($x = 0$). The time of detection of this luminosity serves as zero time for all other measurements. In Figure 11 is shown a sequence of enlarged frames (4x) from the framing camera film. Each frame has two parallel bright bands which represent the backlighting penetrating the spaces between the outside of the tube and the connecting bolts. The semi-circular luminous region at the top of each frame is backlighting above the upper connecting rod. The ignitor is on the left hand side of the frames.

The first frame in Figure 11 shows a luminous zone very close to the ignitor interface (~ 6 mm). It is believed that this zone represents a void that was formed from compaction of the propellant by action of the ignitor gases. This zone appears to propagate at a velocity of ~ 0.03 mm/ μ s for several hundred microseconds. A second luminous zone appears farther downstream as seen in the 284 μ s frame. At 528 μ s the second luminous zone has expanded to cover the entire inner cross section of the tube and has a jagged front, indicative of a convective flame front. We shall call this second luminous zone a convective flame front since its propagation velocity (~ 0.11 mm/ μ sec at 60 mm) and its pressure characteristics are consistent with such an assignment. Figure 12a outlines the propagation paths of the various luminous zones in the x-t plane while Figure 12b shows the strain gage data for four locations.

In the 1259 μ s frame, a distinct dark zone has formed behind the leading edge of the convective flame front. The development of this dark zone can be noted in earlier frames. As time proceeds, the dark zone grows in length and the luminous zone immediately behind the convective front becomes shorter. In the distance-time plane of Figure 12a, the leading edge of the dark zone is seen to be accelerating faster than the convective ignition front. However, the velocity associated with the leading edge of the dark zone (0.33 mm/ μ s) indicates that the dark zone is not propagating at the local sound speed of the porous bed. It should be noted that the last 25 mm at the far end of the charge was not viewed by the camera.

The strain gage data in Figure 12b allow one to determine the time of arrival of pressure (strain) at the various locations as well as to measure the pressure associated with the leading edges of the various fronts. In Table 2 data have been summarized for the leading edges of the luminous CIF from the Lexan experiments; for this experiment the data are for the CIF at three SG locations and the dark zone at two locations. For the convective ignition front, in addition to calculating the velocity and pressure associated with the edge of the luminous front, an induction time τ has also been calculated. The time τ represents the period between arrival of the first detectable pressure (assumed here to represent gas flow)

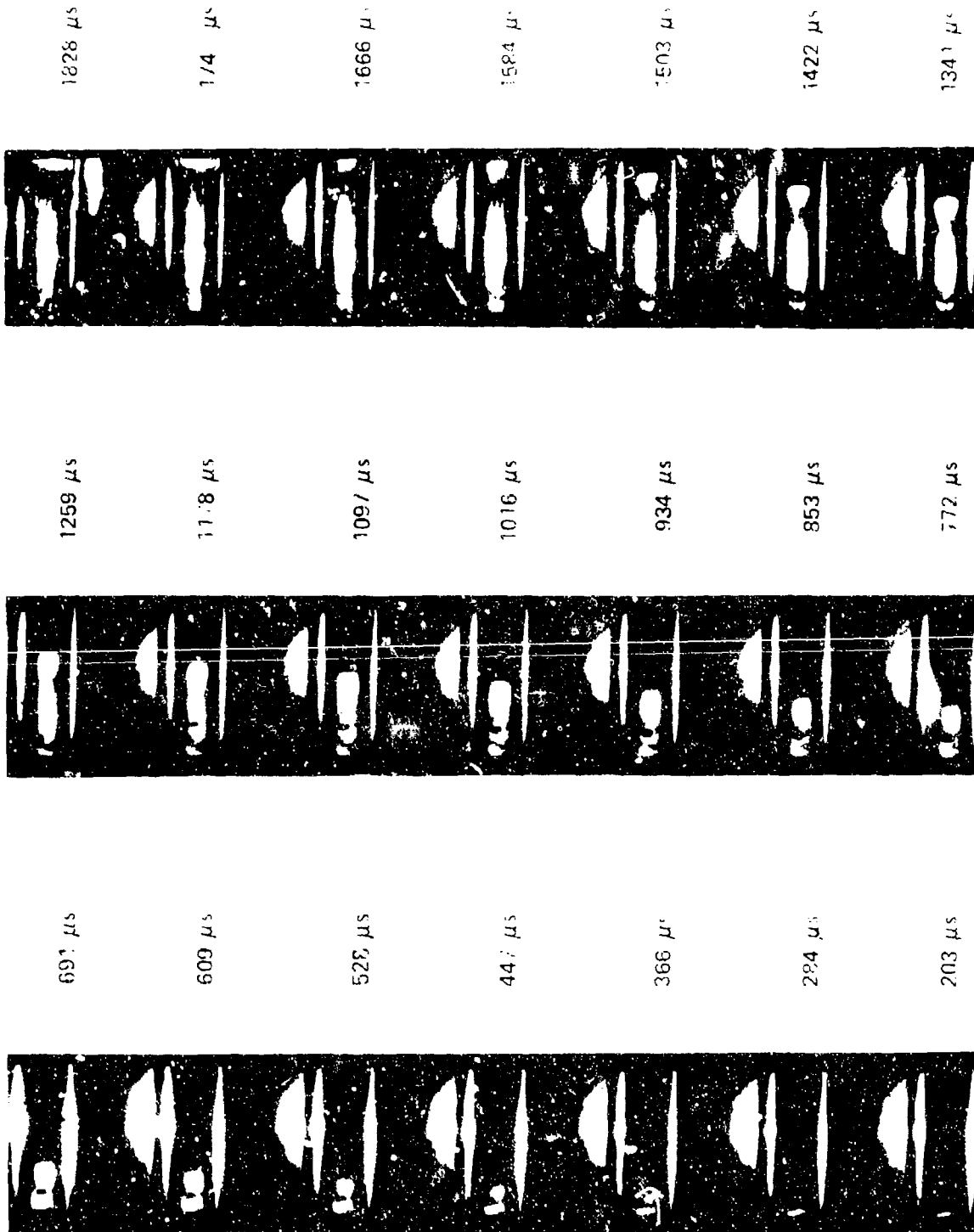
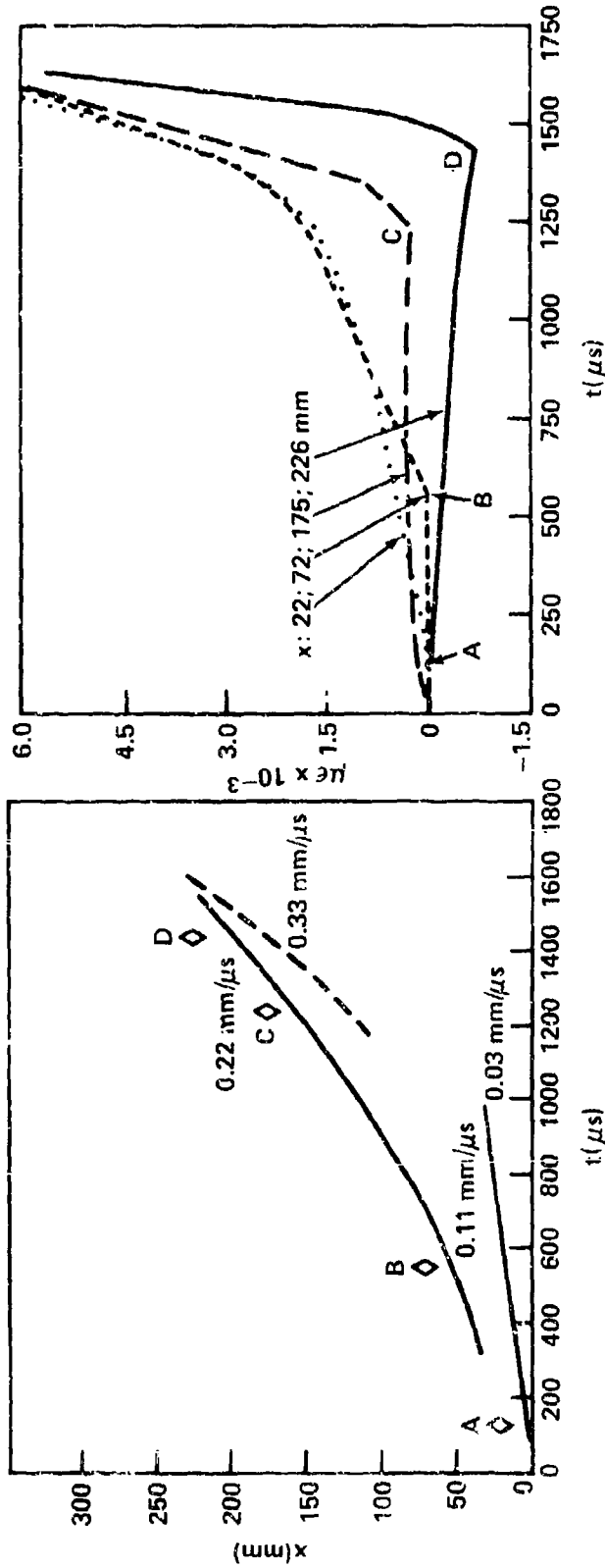


FIGURE 11 SELECTED CAMERA FRAMES FROM SHOT S44 WITH SHREDDED VLU AT 58.5% TMD
 μ_0 110 g cc. (TIME RELATIVE TO RESPONSE OF OPTICAL FIBER ASSEMBLY AT
 IGNITOP INTERFACE FRAMING RATE OF 25,000 fps.)



a. DISTANCE-TIME PLOT (—— EDGE OF LUMINOUS FRONT, - - - EDGE OF DARK ZONE, \diamond FIRST APPEARANCE OF STRAIN FROM ϵ - t CURVE OF b)

b. STRAIN-TIME PLOTS (CHANGE OF SLOPE SHOWN BY LETTERS WHICH ALSO APPEAR IN a)

FIGURE 12 DATA FOR SHOT S44 WITH SHREDDED VLU AT 58.5% TMD, $\rho_0 = 1.10$ g/cc

Table 2. Summary of Predetonation Fronts for Shredded VLU Propellant in Lexan Tube

Front Location mm	Convective Ignition Front				Dark Zone	
	Induction Time, τ μ s	Velocity mm/ μ s	Pressure MPa	Velocity mm/ μ s	Pressure MPa	
<u>Shot S44</u>	(58.5% TMD)					
72	130 (180) ^a	0.12	3 (4) ^a	-	-	
175	110 (160)	0.16	8 (15)	0.32	23 (32) ^a	
226	110 (160)	0.28	20 (40)	0.34	31 (55)	
<u>Shot S45</u>	(58.5% TMD)					
64	145 (195) ^a	0.12	4 (6) ^a	-	-	
<u>Shot S46</u>	(63.8% TMD)					
51	190 (210) ^b	0.16	3 (4) ^b	-	-	
102	~155 (175)	0.21	- ^c	-	-	

a) Upper limit corresponding to time uncertainty (50 μ s) because of interframe interval and transit time through Lexan wall.

b) Correction described in footnote a is only 20 μ s because of conductivity probe correlation.

c) Uncertain because of unknown SG sensitivity setting.

and the first detection of luminosity at a given location as seen by the camera. The luminosity in this case is defined as the time of arrival of the CIF. The value τ is seen to be essentially constant for the three locations between 72 and 226 mm.* However the velocity and the pressure associated with the CIF change dramatically with location along the porous bed. The velocity of the CIF (V_{CIF}) increases by a factor of two between the 72 and 226 mm locations while the associated pressure increases by an order of magnitude. Such a large difference in pressure for the corresponding change in velocity was unexpected.

The dark zone observed in the latter half of the porous column is somewhat puzzling. As expected, the dark zone is associated with a higher pressure than the CIF and the accelerating nature of the dark zone may be associated with the sharpening pressure gradient, dp/dx , at the convective front. More extensive compaction would be associated with the higher pressure of the dark zone and may be responsible for the presence of the dark zone. The increase in luminosity behind the dark zone (closer to the ignition region) would then indicate a decrease in density (due to consumption of the propellant) or flame propagation down annular spaces formed between expanding walls and the compacted charge.

To extend our knowledge of the convective ignition front and the dark zone observed in Shot S44, a second experiment was prepared; the column length was increased to 289.0 mm and SG locations were moved farther from the ignition region. Unexpectedly a transition to detonation occurred, with quite dissimilar predetonation events. Selected frames (10x magnification) from Shot S45 are shown in Figure 13. The initial frames (not shown) showed a slowly propagating luminous zone similar to that discussed in Shot S44.

A second luminous zone began to develop at $\sim 520 \mu s$. It can be seen clearly in the 680 μs frame of Figure 13. This second zone of luminosity developed as a peninsula that primarily penetrated axially rather than both axially and laterally as in the previous experiment. This second zone again appears to be a convective flame front; its velocity is essentially constant and is 0.12 mm/ μs as shown in the distance-time plane of Figure 14a.

*The values of τ have been calculated with the assumption that the backlighting (time fiducial for the camera) appeared at the instant the frame was taken. However, the backlighting can appear just after a frame is taken also. Thus, there can be a synchronization error between the SG data and the camera frames equal to the approximate interframe time, 40 μs , plus the transit time for waves to travel through the Lexan wall (25.4 mm thick). Consequently the total time error can be about 50 μs . The data in parentheses in Table 2 represent maximum corrections for any time difference.

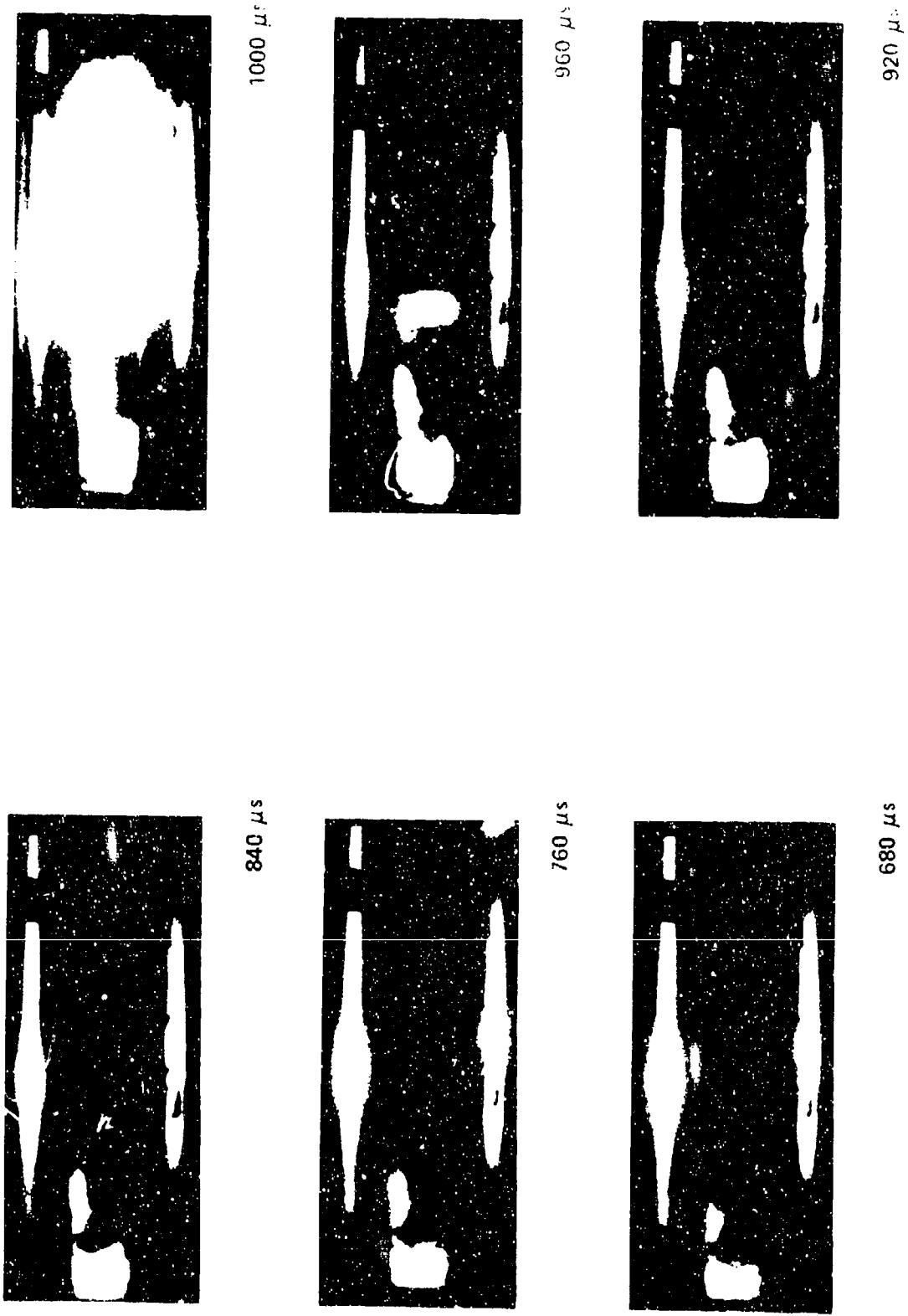
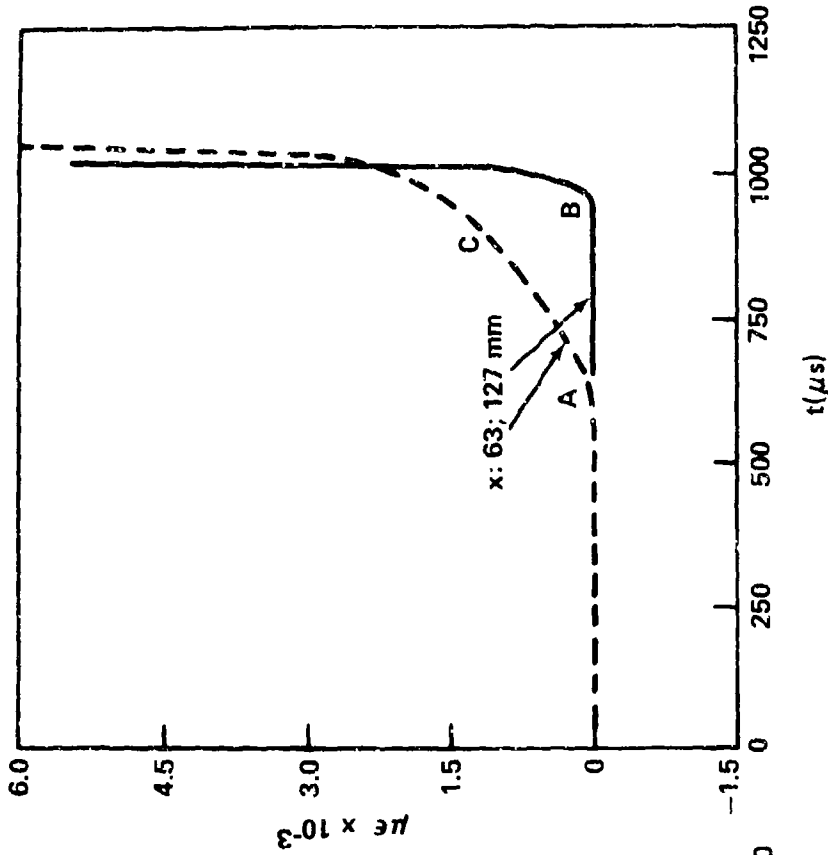


FIGURE 13 SELECTED CAMERA FRAMES FROM SHOT S45 WITH SHREDDED VLU AT 58.5% TMD.
 $\rho_0 = 1.10$ g/cc. (KEY OF FIGURE 9)

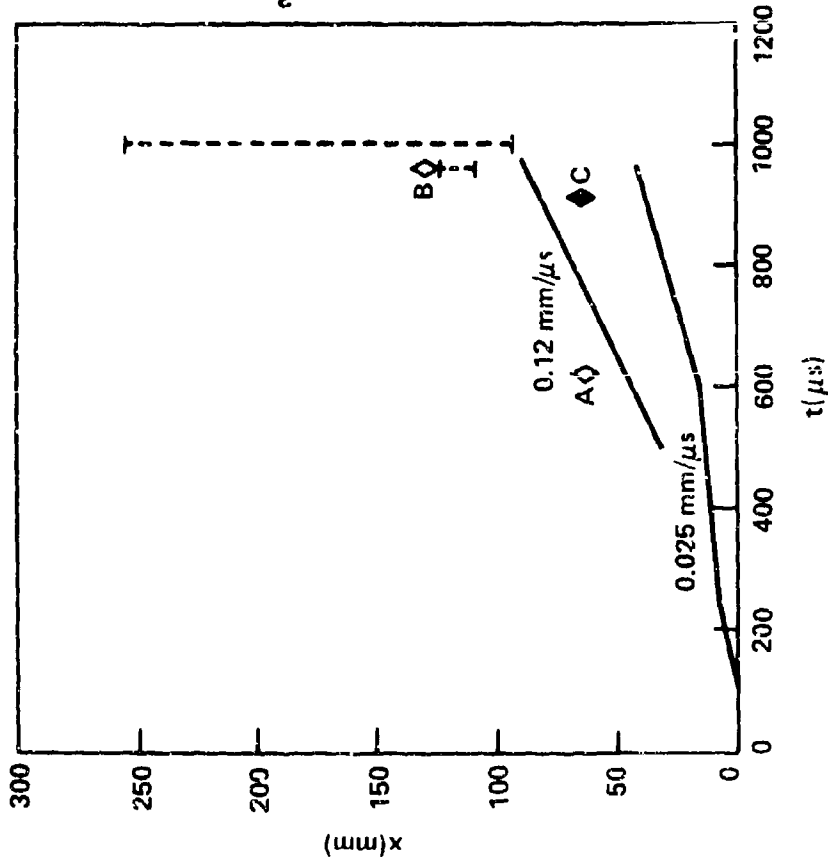
An abrupt change in the luminous pattern is noted in the 960 μ s frame in Figure 13. A bright band, extending from 108 mm to 123 mm, is seen approximately 20 mm ahead of the convective flame front. This new bright zone (band) may have arisen from penetration of combustion by a path that is not visible. However, it is somewhat difficult to account for the planarity, at the ends of this new luminous band, with a convective combustion mechanism. It is tempting to evoke some other mechanism, e.g., a thermal explosion, especially since a transition to detonation occurs shortly thereafter. In the 1000 μ s frame it appears that a transition to detonation has occurred or is very near to occurring. Between 960 and 1000 μ s the luminous front has an average velocity of 3.3 mm/ μ s. Thus detonation did not begin before 960 μ s.

Limited information was obtained from the SG data (Figure 14b) since only two locations were in the predetonation column. Fortunately, one of those locations (127 mm) was very close to the head of the bright band seen in the 960 μ s frame. It is evident from Figure 14b that pressure buildup at 127 mm is rapid after 950 μ s, when pressure first appeared at that location. At the other (63 mm) location, pressure was first detected at 615 μ s. At later times ($< 1025 \mu$ s) pressure increases but with a pressurization rate of 140 GPa/s (1.4×10^6 atm/s) or less; this rate is associated with a convective combustion wave. Hence both the SG and camera data point to a thermal explosion-like event as the driving force for a transit to detonation.

A third experiment (Shot S46) was fired with shredded VLU in the Lexan tube; it utilized a 63.8 %TMD charge. Based upon damage to the end plate as well as conductivity probe data, a transition to detonation occurred. Figure 15 shows selected frames from the camera film; the initial luminous events, as summarized in the distance-time plane of Figure 16a, were quite similar to those from Shots S44 and S45. The nature of the propagating convective ignition front is intermediate in behavior, compared to the two 58.5 %TMD Lexan experiments. That is, the CIF initially propagated preferentially down one side but spread both axially and laterally thereafter. In the 955 and 1000 μ s frames, it is interesting to note the planarity of the head of the luminous front. From Figure 16a, one sees that these planar fronts are associated with a compressive wave whose apparent velocity is 1.4 mm/ μ s. A transition to detonation occurred before the next (1045 μ s) frame; in Figure 16a, conductivity probe data outline a detonation front between 248 and 273 mm. The predetonation column length is estimated to be between 180 and 210 mm. The SG data of Figure 16 show a pattern consistent with Shot S45; data for the convective flame front are listed also in Table 2. The parameters for the CIF in the earlier region of the predetonation column appear to be remarkably similar in all three experiments.



a. DISTANCE-TIME PLOT (—— EDGE OF LUMINOUS FRONT, - - - UNIQUE LUMINOUS ZONE, \diamond FIRST APPEARANCE OF STRAIN FROM ϵ - t CURVE OF b, \diamond LATER CHANGE IN SLOPE OF ϵ - t CURVE OF b)



b. STRAIN-TIME PLOTS (CHANGE OF SLOPE SHOWN BY LETTERS WHICH ALSO APPEAR IN a)

FIGURE 14 DATA FOR SHOT S45 WITH SHREDDED VLU AT 58.5% TMD, $\rho_0 = 1.10 \text{ g/cc}$



818 μ s



727 μ s



636 μ s



1000 μ s

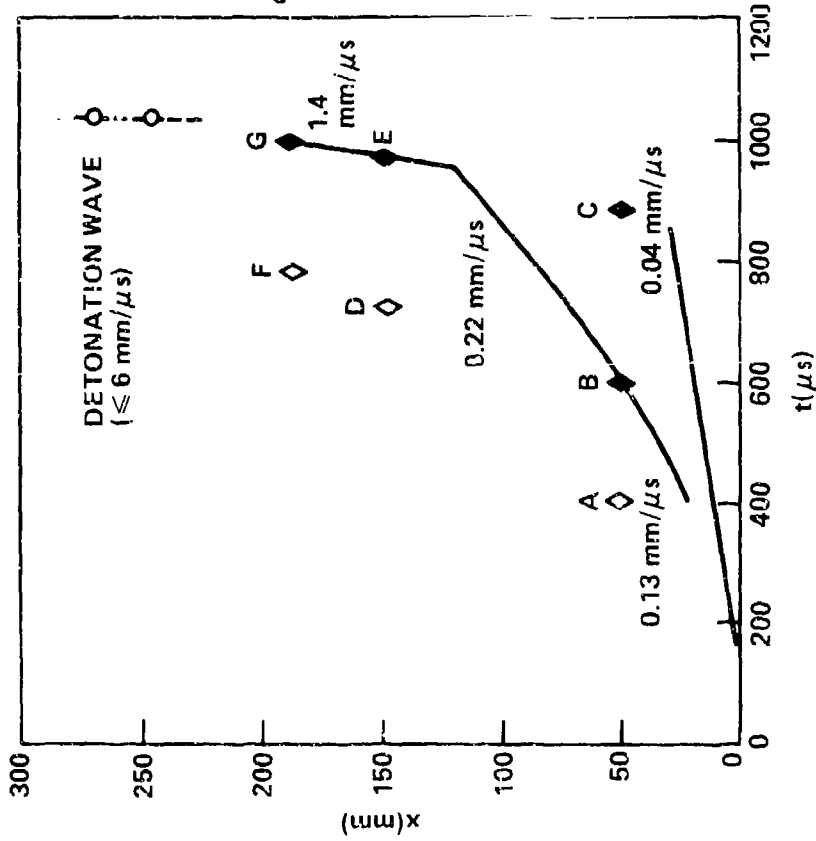


955 μ s

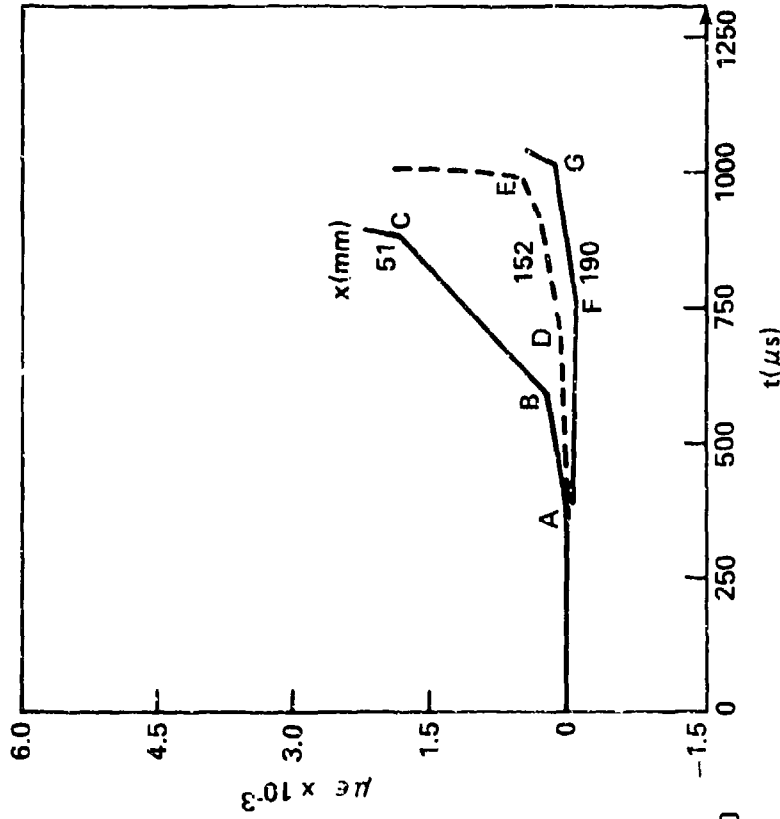


909 μ s

FIGURE 15 SELECTED CAMERA FRAMES FROM SHOT S46 WITH SHREDDED VLU AT 63.8% TMD,
 $\rho_0 = 1.2$ g/cc. (TIME RELATIVE TO RESPONSE OF OPTICAL FIBER ASSEMBLY AT
 IGNITOR INTERFACE; FRAMING RATE OF 22,000 fps.)



a. DISTANCE-TIME PLOT (--- EDGE OF LUMINOUS FRONT, \blacklozenge FIRST APPEARANCE OF STRAIN FROM ϵ - t CURVE OF b, \blacklozenge LATER CHANGE IN SLOPE OF ϵ - t CURVE OF b, \bullet RESPONSE OF CONDUCTIVITY PROBE)



b. STRAIN-TIME PLOTS (CHANGE OF SLOPE SHOWN BY LETTERS WHICH ALSO APPEAR IN a)

FIGURE 16 DATA FOR SHOT S46 WITH SHREDDED VLU AT 63.8% TMD, $\rho_0 = 1.20$ g/cc

SUMMARY AND CONCLUSIONS OF DDT EXPERIMENTS WITH
VLU PROPELLANT

DDT experiments at both high and low confinement have demonstrated that the region of accelerating pressure buildup, necessary for a transition to detonation, occurred shortly before (both in time and distance) the onset of detonation. The origin of the event producing the accelerated buildup is unknown but is indicative of a rapid heat release mechanism (e.g., a thermal explosion) rather than a pressure buildup produced by confined (convective) burning. The DDT characteristics observed here for the porous VLU propellant columns are quite similar to those observed for tetryl.¹²

Experiments conducted in the low confinement (Lexan) system have provided parameters associated with the convective ignition front; these parameters should be useful in checking calculations concerning the CIF from numerical models of DDT. Compaction, which is present during all the stages of the DDT process, must also be considered in the interpretation of the CIF parameters observed in these experiments. Compaction during the early stages is illustrated by the slow luminous fronts (~ 0.04 mm/ μ sec) seen in Figures 12a, 14a, and 16a. More detailed discussion of the compaction process in XLDB propellants is presented elsewhere.¹¹

The predetonation column lengths observed in the high confinement (steel tube) and low confinement (Lexan tube) systems at high porosities are comparable, as shown in Table 3.

Table 3. Summary of DDT Experiments with Shredded Porous Propellant

Propellant	Shot No.	Density g/cc	%TMD	λ (mm)	
				Steel ^a	Lexan ^b
VLU	S45	1.10	58.5	168	150-170
VLU	S46	1.20	63.8	168	180-210

a) ID/OD: 16.7 mm/50.8 mm; λ derived from smoothed curve of Figure 8.

b) ID/OD: 25.4 mm/76.2 mm

It is not as easy to compare the relative times to detonation in the two confinements. Shots S45 and S46 had a total time to onset of detonation t_D (from first luminosity and from $x = 0$) of 1000 and 1030 μs , respectively. From Figs. 14 and 16, the respective times for a disturbance to reach $x = 41$ mm are 550 and 543 μs . Thus the times referred to $x = 41$ are 450 and 487 μs , respectively. They can be compared to $4l\Delta t_D$ of 247 and 230 μs from Fig. 9. Thus the relative times to detonation seem to be the same order of magnitude in the two experimental configurations. Still unresolved is the quantitative relationship between luminosity detected by the optical fibers and the conductivity which causes the IP response. Also, still to be determined is the diameter effect on the entire transitional process.

Thus, the effect of confinement on the DDT susceptibility of this material at high porosity is small; this is in agreement with the deduced physical mechanism. That is, confinement would be expected to play a minor role if pressure buildup and tube deformation along most of the predetonation column length is relatively low and the accelerating pressure buildup necessary for DDT occurs shortly before the onset of detonation.* It is expected that confinement would be more important at lower porosities (higher %TMD).

* The effect of charge diameter on λ values for this propellant, has not been explored. However, for data from other explosive experiments the effect appears minimal in steel tubes with ID/OD ratios of 16.7/50.8 and 25.4/76.2.

REFERENCES

1. Belyaev, A. F., Bobolev, V. K., Korotkov, A. I., Sulimov, A. A., and Chuiko, S. V., "Transition from Deflagration to Detonation in Condensed Phases," Izdatel'stvo "Nauka", Moscow, 1973 through Israel Program for Scientific Translations 1975.
- 2a. Bernecker, R. R. and Price, D., "Studies in the Transition from Deflagration to Detonation in Granular Explosives. II. Transitional Characteristics and Mechanisms Observed in 91/9 RDX/wax." Comb. and Flame, 22, 119 (1974). See also NOLTR 72-202.
- b. Bernecker, R. R. and Price, D., "Studies in the Transition from Deflagration to Detonation in Granular Explosives. I. Experimental Arrangement and Behavior of Explosives which Fail to Exhibit Detonation," Comb. and Flame, 22, 111 (1974). See also NOLTR 72-202.
3. Korotkov, A. I., Sulimov, A. A., Obmenin, A. V., Dubovitskiĭ, V. F., and Kurkin, A. I., "Transition from Combustion to Detonation in Porous Explosives," Combustion, Explosion and Shock Waves, 5, (3) 315-325 (1969).
4. Bernecker, R. R. and Price, D., "burning to Detonation Transition in Picric Acid," Seventeenth Symposium (International) on Combustion. Combustion Institute, 1979; pp 55-61. See also NSWC/WOL/TR 76-31 and 77-175.
5. Hyndman, J. R., Brandon, W. W., and Shuey, H. M., "Deflagration-Detonation Studies of Solid Propellants," presented at Twelfth Meeting of the JANNAF Solid Propellant Group, Silver Spring, Maryland, 7 May 1956.
6. Hyndman, J. R. and Brandon, W. W., "Deflagration to Detonation Transition in Solid Propellants: An Experimental Study," presented at Thirteenth Meeting of the JANNAF Solid Propellant Group, Chicago, Illinois, 4 June 1957.
7. Pilcher, D. T., Beckstead, M. W., Christensen, L. W. and King, A. J., "Comparison of Model Predictions and Experimental Results of DDT Tests," AIAA/SAE 13th Joint Propulsion Conference, Orlando, Florida, 11 July 1977.
8. Butcher, A. G., Hopkins, B. D., Robinson, N. J., and Beckstead, M. W., "Fundamental Experiments on DDT," presented at 15th JANNAF Combustion Meeting, Newport, Rhode Island 11 September 1978.

9. Sandusky, H. W. and Bernecker, R. R., "Transparent Tube Studies of Burning to Detonation Transition in Granular Explosives. I. Preliminary Framing Camera Results," Naval Surface Weapons Center Report NSWC/TR 79-79, to be published.
10. Price, D. and Bernecker, R. R., "DDT Behavior of Ground Tetryl and Picric Acid," Naval Surface Weapons Center Report NSWC/WOL/TR 77-175, 25 January 1978.
11. Bernecker, R. R., Sandusky, H. W. and Clairmont, A. R., Jr., "Compaction and the Burning to Detonation Transition at Low Confinement." presented at Sixteenth JANNAF Combustion Meeting, Monterey, California, 10 September 1979.
12. Bernecker, R. R., Price, D., Erkman, J. O., and Clairmont, A. R., Jr., "Deflagration to Detonation Transition Behavior of Tetryl," Sixth Symposium (International) on Detonation, San Diego, California (1976), P. 426. See Also NSWC/WOL/TR 76-31.
13. Price, D. and Bernecker, R. R., "Effect of Wax on the Deflagration to Detonation Transition of Porous Explosives," Proceedings of Symposium (International) on High Dynamic Pressure in Paris, CEA, Soclay, France, 1978; pp. 149-159. See also NSWC/WOL TR 77-96.
14. Ashchepkov, N. V. and Sten'gach, V. V., "Predetonation Section of the Combustion-Detonation Transition in PETN" Combustion, Explosion and Shock Waves, 10 (6), 783-786 (1974).

APPENDIX A

ADDITIONAL DATA

Detailed data for all shots on VLU-10 are given in this section.

Shredded VLU

Data for the charges prepared from the shredded VLU are given in Table A1 and displayed in Figs. A1-A9.

Fig. A1 for 90.5% TMD charge shows an initial 0.3 mm/ μ s flame front that smoothly accelerates until the onset of detonation at 452 μ s. The initial velocity is about that observed in many convective flame fronts; however, the SG records give no indication of a subsequent post-convective (compression) front. The detonation velocity is a bit low for this charge density, but reasonable since the value was obtained from only two IPs.

To obtain the necessary predetonation length for transition in this charge, the usual tube length was doubled; the interface between the two pieces of tubing used is indicated in Fig. A1a. The rearward compression wave travelling at 3.9 mm/ μ s might be a reflection (of an undetected disturbance) from that interface or it might be from an explosive event that sent out both forward and rearward waves. In the latter case, the forward disturbance could not have been observed because no SGs were mounted on the farther length of tubing. The 3.9 mm/ μ s front was not generated by the onset of detonation because it occurs too early to have been caused at that time (Δt_p).

The 86.6% TMD charge was also fired in a double length tube (Fig. A2). The front outlined by the IPs seemed of constant velocity at 0.45 mm/ μ s rather than accelerating (This is possibly an artifact caused by an early discharge of the second IP.) In this case, a thermal explosion might have occurred at about 184 mm where both forward and rearward traveling compressive waves (\sim 2.6 mm/ μ s) might have originated. The forward traveling compression does not resemble a PC wave such as those repeatedly observed in 91/9 RDX/wax.² The detonation velocity, established by the discharge of seven IPs is that to be expected at this density.

Fig. A3 for the 82.6% TMD shows an IP front which appears to be accelerating smoothly from an initial velocity of 0.13 mm/ μ s. At this porosity we first see difficulties with the response of the IPs; subsequent shots show that such difficulties are enhanced as the porosity increases. Here the second IP did not respond at all and the third IP seems to have responded late; even the fifth

IP showed only a partial discharge. However, enough of the record was obtained to indicate smooth acceleration to a detonation velocity about 10% below that estimated for this density. At the same time, no PC wave was evident. On the other hand, we have the first example of what is called the "steel wave" in the text. It is a mild compressive wave that appears to originate at the point of onset of detonation and travels rearward at a velocity about the same as that of the detonation. In this case, it is about 10% lower but in most of the other cases (presented below) it is 10% or more higher.

Fig. A4 displays the data for the 78.7% TMD charge, the same data as those of Fig. 7 in the text. The only addition here is of the partial discharges of the 2nd and 3rd IP shown in Fig. A4a; they further confirm the constant velocity of the initial IP front. Again no PC wave is evident and the "steel wave" is a mild compressive disturbance traveling rearward; it extrapolates back to the point of detonation onset.

Shot 817 at 74.6% TMD did not transit to detonation. Fig. A5a shows an IP front smoothly accelerating from 0.12 to 0.3 mm/ μ s. It then showed a constant velocity over the next 60 mm after which it failed to activate the next IP. The subsequent and final IP did respond to show a final velocity of 0.9 mm/ μ s. The response pattern is similar to that of Shot 802 (Fig. A3) where the second IP failed to respond and the third seemed to have a late response. It is possible that the last probe in Fig. A5a also had a late response, and that the final velocity was actually greater than 0.9 mm/ μ s. Strain-time records were obtained only for the last three SGs and only one of these (that for the last SG at 156 mm) exhibited an excursion. However, both the higher final velocity and the pressure excursion at 156 mm suggest the occurrence of some event which might have led to a transition had the charge been longer. Lack of a dent in the closure bolt and the large tube fragments indicated that detonation had not been achieved by the time the disturbance reached the end of the tube.

Fig. A6 is also for a 74.5% TMD charge which did undergo transition although neither of the first two IPs showed any response. The pre-detonation pressure excursions suggest an explosive event at $x = 119$ mm leading at 149 mm to detonation (6.1 mm/ μ s, a rate expected at this density). The "steel wave" in this case travels rearward at 6.5 mm/ μ s, somewhat faster than the detonation wave.

A very similar pattern was obtained for the 70.7% TMD charge. This is illustrated in Fig. 6 of the text where that shot (No. 804) is discussed.

Records for the shot on the 54.4% TMD charge (Fig. A7) show the usual problem of IP discharge in the high porosity VLU as well as the additional complication of uncertainty in assigning measured response time to the appropriate probe. However, there is no doubt that the charge showed a transition and detonated at an appropriate rate for its density. The rearward traveling compressive wave is too slow for

a "steel wave", and is more apt to have resulted from an explosive event; no SGs were in a position to monitor any forward traveling wave from such an event.

By way of contrast, the 60.4% TMD charge of Fig. A8 shows four IPs that did not respond and a "steel wave" of about 7 mm/ μ s compared to a detonation velocity of 5. The final charge of this series was at 54.3% TMD. Its data are displayed in Fig. A9. Note that Fig. A9a is Fig. 4 of the text.

Powdered VLU

Data for the charges prepared from the powdered VLU are given in Table A2 and displayed in Figs. A10 - A13.

Fig. A10 for an 86.2% TMD charge shows three inactive IPs, an IP front initially nominally at 0.64 mm/ μ s,* followed by a 1.5 mm/ μ s compression front. The last, like those observed in the records of shredded VLU, appears to originate at some distance from the ignitor, i.e., the first two SGs give no indication of this front. The onset of detonation at 6.94 mm/ μ s terminates a smooth acceleration of the IP front and seems influenced by the observed compressive front only to the extent of moderately increasing the velocity.

In contrast to the 86.2% TMD charge, the 83.8% TMD charge showed IP response problems only with a double discharge of the first probe and possibly a late response of the third (see Fig. A11a). It exhibited a weak,** 0.59 mm/ μ s compressive front that was detected by the first SG, but it also showed a stronger, rearward traveling, 2.6 mm/ μ s compression front that suggests a companion forward traveling front (undetected), both caused by some explosive event. The late pressure excursion at $x = 67$ mm might well be a portion of the "steel wave".

The 74.1% TMD charge of Fig. A12 exhibits the same patterns as those shown by the 83.8% TMD charge with the exception that the first mild compression wave was not detected on the first two SGs. Thus, it resembles most of the other charges in this respect, and it is the 86.2% TMD which is unusual.

The 65.4% TMD charge (Fig. A13) exhibited much the same behavior although no "steel wave" was detected. Up to onset of detonation, SGs registered a maximum of one kbar. The 53.7% TMD charge was discussed in the main text; its data are displayed there in Fig. 5 and will not be further discussed here.

*This velocity is about twice the average value for most of the other shots, and together with the unresponsive IPs, indicates a much too late discharge of the first IP.

**Up to 400 μ s, all SGs except the first registered less than 1.6 kbar. Probably this is the pressure front associated with the convective flame front.

VLU Cubes and Slugs (Table A3)

Shot 1104 was made on 1/16 inch cubes of VLU packed to 59.6% TMU. As Fig. A14 shows, this material did transit. Three IPs failed to function; the remainder indicated an initial front of about 0.8 mm/ μ s. It was followed by a low pressure front at 2.4 mm/ μ s. Up to 110 μ s, no SG registered more than about one kbar, hence this front might be traveling for the most part through the solid cubes at the sound velocity of the voidless material. At about 115 μ s, however, the last SG (at $x = 181$ mm) showed a rapid pressure rise to the yield point of the steel tube in the next 10 μ s, after which pressure continued increasing at the accelerated rate. Consequently, the pressure front sent forward from $x = 181$ mm is much stronger than the earlier front; it also shows a rearward traveling branch indicating the occurrence of an explosive event. About 30 μ s after the stronger front was detected, detonation occurred about 50 mm downstream. The "steel wave" in this case seemed to originate from the high pressure region about 25 mm ahead of the location of the point of onset; it traveled at about 5.6 mm/ μ s compared to the detonation velocity of 5.0 mm/ μ s.

The 1/8 inch cubes were packed to approximately the same porosity, but the nature of the reactions after ignition was such that only a few IPs responded, and no transition occurred. Thus our records are entirely from the SGs. As Fig. A15 shows, the tube became uniformly pressurized about 180 μ s after response of the triggering IP. At 300 μ s, a strong (nominally over 5 kbar) compression front has formed and moved down the tube at a shock velocity. It dispersed with failure of the end closure of the tube and rapid escape of the high pressure gas.

Slugs of VLU-10 (0.63 \pm 0.003 in. dia x 2.0 in. long) were used in an attempt to fill a DDT tube with voidless propellant. A "slip fit" procedure at dry ice temperature, recommended by Hercules Bacchus, was used. Inasmuch as the slugs were not of uniform diameter and showed plastic deformation even at dry ice temperature, the attempt was more of a "push-fit" and was not successful. The xray of the loading finally obtained showed a gap of 0.04 in. at 51.3 mm and a long void at $x = 151.4-169.4$ mm.

Although this charge failed to transit, it burned completely, i.e. no solid residue was found after the shot. The first probe to respond after ignition was at 54.1 mm, i.e. beyond the interface gap; the location of the longitudinal void is indicated on Fig. A16a. The initial 0.27 mm/ μ s IP front ran for about 200 μ s after which it was slowed down or disappeared. At 338 μ s a faster front appeared. It initially traveled at 2.5 mm/ μ s but decelerated to about 0.6 mm/ μ s between the last two IPs. At about the time the faster front was detected, a mild compression wave was also detected in the same region; it traveled rearward. The same event might be responsible for both the faster IP front and the rearward traveling wave; its location seemed near the longitudinal void, but that appeared to have little effect on the IP front.

Although the strains shown in Fig. A15b reached as large values as those of Fig. A15a (1/8 in. cubes), the rate of pressure increase was much less. Either for this reason or because the interpretation of ϵ -t records is more complex when transmission is through a solid medium, this tube was split in half whereas that containing the 1/8 in. cubes was relatively undamaged because the end closure was blown off. The first, third, and fourth SG stopped functioning between 600 μ s (the fourth) and 740 μ s (first), whereas the second and fifth SG functioned until 840 and 760 μ s, respectively.

Detonation Velocity

Although the DDT experiments are not well designed to measure the detonation velocity D accurately, we do obtain D values whenever transition occurs early enough. The values of Tables A1 and A2 for s and p VLU-10 have been plotted in Fig. A15. The lines drawn are heavily weighted by the D values with $\sigma \leq 0.2$ mm/ μ s. From these data,

$$D \text{ (mm}/\mu\text{s)} = 0.80 + 0.0726 (\%TMD) \quad p\text{VLU-10}$$

$$D \text{ (mm}/\mu\text{s)} = 0.60 + 0.0727 (\%TMD) \quad s\text{VLU-10}$$

The above equations give D values of 8.06 and 7.97 mm/ μ s for the voidless material at 1.88 g/cm³.

TABLE A1
DETAILED DATA FOR SHREDDED VLU-10

Shot No.	1001		902		802	
Density: (g/cm ³)	1.705		1.629		1.553	
(%TMD)**	90.7		86.6		82.6	
IP Data	<u>x</u>	<u>t</u>	<u>x</u>	<u>t</u>	<u>x</u>	<u>t</u>
	41.5	Bad pin*	41.4	0.0*	28.7	0.0*
	79.6	0.0*	92.2	87.4*	54.2	-
	117.7	120.1*	143.1	250.3*	66.9	481.1*
	171.4	252.15*	193.8	338.7*	79.6	403.1*
	215.6	315.65*	232.0	347.1*	104.9	546.4*
	253.9	373.3*	257.3	350.3*	130.4	613.6*
	292.1	415.0*	311.0	357.1*	155.8	659.4*
	323.8	439.4*	349.1	362.8*	181.2	681.6*
	355.5	450.6*	387.2	367.7*	206.6	690.4*
	387.3	455.2*	425.2	373.0*	257.4	698.8*
	425.4	461.2*	526.9	388.2*		
Strain Gage Data	<u>x</u>	<u>t</u>	<u>x</u>	<u>t</u>	<u>x</u>	<u>t</u>
	20.7	513-522	20.7	389	20.6	720
	92.5	500	155.8	336-345	54.6	704
	194.3	474	194.1	322	79.8	694,709
	219.5	468	232.0	349	174.9	697
	245.4	458			130.7	690
Predetonation vel., mm/ μ s	0.3 - 1.3		~0.45		0.13 - 1.6	
Predetonation Column Length ^a (mm)	>359, (355 ⁺⁵ -0)		(232 \pm 5)		(206 \pm 10)	
⁴¹ Δt_D (μ s)	-		347		590	
¹⁵⁶ Δt_D (μ s)	231		73		30	
D(σ), mm/ μ s	6.58(0.16) much of tube intact		7.19(0.11)		>6.05(-)	

*Custom made probes.

** $\rho_v = 1.88$ g/cm³.

a. Values in parentheses determined from IP data.

Units of x and t are mm and μ s respectively.

TABLE A1 (Cont'd)

DETAILED DATA FOR SHREDDED VLU-10

Shot No.	803		817		712	
Density: (g/cm ³)	1.47 ₇		1.40 ₂		1.399	
(%TMD)**	78.6		74.6		74.4	
IP Data	<u>x</u>	<u>t</u>	<u>x</u>	<u>t</u>	<u>x</u>	<u>t</u>
	41.4	0.0*	41.4	0.0*	41.4	-*
	66.3	(49.5)*	79.5	319.6*	54.2	-*
	92.0	(106.2)*	104.9	472.4*	79.6	0.0*
	117.6	158.3*	124.0	576.0*	105.0	114.8*
	143.0	219.8*	143.0	663.7*	130.4	140.6*
	155.7	244.5*	162.1	735.8*	155.8	149.1*
	174.6	253.3*	181.2	798.9*	181.2	152.0*
	193.8	260.4*	200.2	864.7*	206.5	156.9*
	212.9	263.0*	219.2	921.4*	232.0	160.0*
	231.9	267.4*	238.3	-*	257.4	165.2*
	257.1	270.6*	257.3	963.3*	295.4	171.0*
Strain Gage Data	<u>x</u>	<u>t</u>	<u>x</u>	<u>t</u>	<u>x</u>	<u>t</u>
	20.6	~237	20.4	-	20.3	167
	117.9	~271	79.4	-	54.5	164
	143.3	232	105.0	-	79.5	159
	162.6	239	130.4	-	105.2	138?, 146
	181.5	249	155.8	992	130.3	138
Predetonation vel., mm/μs	0.46, 2.2		0.2 - 0.9		0.22 - 0.98	
Predetonation Column Length ^a (mm)	>163, (188 ⁺⁵ -2)		-		149(147±8)	
⁴¹ Δt _D (μs)	269		-		-	
¹⁵⁶ Δt _D (μs)	25		-		-	
D(σ), mm/μs	5.92 (0.50)		F		6.10 (0.38)	

*Custom made probes.

**ρ_V = 1.88 g/cm³

a. Values in parentheses determined from IP data.

Units of x and t are mm and μs respectively.

TABLE A1 (Cont'd)

DETAILED DATA FOR SHREDED VLU-10

Shot No.	804		710		901		709	
Density: (g/cm ³)	1.326		1.209		1.136		1.018	
(%TMD)**	70.5		64.3		60.4		54.1	
IP Data	<u>x</u>	<u>t</u>	<u>x</u>	<u>t</u>	<u>x</u>	<u>t</u>	<u>x</u>	<u>t</u>
	41.4	-*b	41.5	-*	41.4	-*	34.0	-*
	66.8	-*	54.1	-*	79.5	-*	54.2	-*
	92.2	0.0*	79.6	0.0(?)*	104.9	-*	79.6	-*
	117.6	80.2*	104.9	68.9*	124.0	-*	117.7	-*
	143.0	-*	130.4	198(?)*	143.0	0.0	155.2	0.0*
	155.7	147.3*	155.8	82.35*	162.1	8.4*	181.4	7.8*
	174.8	153.8*	181.2	177.0*	181.1	14.2*	206.8	13.9*
	193.8	157.5*	206.5	184.7*	200.2	17.85*	232.2	18.8*
	212.9	160.9*	232.0	190.0*	219.2	21.9*	257.6	25.0*
	231.9	163.7*	257.4	194.15*	238.3	25.25*		
	257.3	168.7*			257.3	29.35*		
Strain Gage Data	<u>x</u>	<u>t</u>	<u>x</u>	<u>t</u>	<u>x</u>	<u>t</u>	<u>x</u>	<u>t</u>
	20.4	172	20.4	241	20.7	32	20.2	25.0
	92.6	145-170	60.7	183,223	92.2	26.7	53.8	4.8
	117.9	152	79.4	173,213	117.6	18.7,21.8	79.2	-
	137.0	141	98.9	168,195	137.0	18.3,15.2	104.6	-
	155.7	142	118.1	188	156.1	12.6,16.6	130.2	-
Predetonation vel., mm/ μ s	0.34		0.27		2.27		-	
Predetonation Column Length ^a (mm)	(170 \pm 10)		194 \pm 6		168(170 \pm 3)		172 \pm 6	
⁴¹ Δt_D (μ s)	-		-		-		-	
¹⁵⁶ Δt_D (μ s)	5.4		100		6.3		6.0	
D(σ), mm/ μ s	5.62(0.14)		5.36(0.37)		5.05(0.09)		4.49(0.14)	

*Custom made probes.

** $\rho_V = 1.88$ g/cm³.

a. Values in parenthesis determined from IP data; b. probe had NC deposited on its tip.

Units of x and t are mm and μ s, respectively.

TABLE A2

DETAILED DATA FOR POWDERED VLU-10

Shot No.	1219		1201		1016	
Density: g/cm^3	1.621		1.576		1.402	
%TMD**	86.2		83.8		74.6	
IP Data	<u>x</u>	<u>t</u>	<u>x</u>	<u>t</u>	<u>x</u>	<u>t</u>
	41.3	0.0*	41.4	0.0, 24.2*	28.8	- ^b
	60.3	-*	66.9	212.85*	41.5	-*
	79.4	-*	92.3	360.4*	60.7	0.0*
	104.8	-*	117.6	316.15*	79.8	94.1*
	130.2	136.7*	143.0	369.4*	98.7	179.3*
	155.6	180.4*	168.5	406.8*	117.9	229.6*
	181.1	211.2*	187.6	432.3*	143.3	282.0*
	206.5	225.7*	206.6	438.5*	168.7	294.6*
	225.4	230.4*	225.7	442.1*	194.2	298.1*
	244.6	233.9*	244.7	444.8*	219.5	302.9*
	263.7	235.75*	263.8	448.25*	244.9	306.4*
					263.9	309.8*
SG Data	66.9	-	66.9	200,486	20.6	- , 315
	143.1	-	136.9	316-330,457	67.7	- , 308
	168.5	180,194	156.0	350,443	92.3	120,313
	187.6	194,210	175.0	387,411	117.9	202,293
	205.5	220,230	194.1	420,-	143.8	256,280
Predetonation vel., mm/ μs	0.64 - 1.75, 1.5		0.12, 0.59		0.20 - 0.60	
λ (mm)	222		214		166	
$^{41}\Delta t_D$ (μs)	-		440		364-372 (extrap)	
$^{156}\Delta t_D$ (μs)	45		37		6	
$D^{(0)}$ mm/ μs	6.94(0.45)		6.17(0.42)		6.22(0.18)	

*Custom-made probes.

** $\rho_V = 1.88 \text{ g/cm}^3$.

a. Values in parentheses from IP record.

b. Conductivity probe.

Units of x and t are mm and μs , respectively.

TABLE A2 (Cont'd)

DETAILED DATA FOR POWDERED VLU-10

Shot No.	1211		1217	
Density: g/cm^3	1.233		1.011	
%TMD**	65.4		53.7	
IP Data	<u>x</u>	<u>t</u>	<u>x</u>	<u>t</u>
	28.4	0.0 ^b	41.7	0.0 ^b
	41.0	149.0*	54.4	-*
	60.1	240.5*	79.2	129.5*
	79.2	283.2*	105.2	215.85*
	104.6	341.75*	130.4	259.75*
	130.0	376.05*	156.0	267.0*
	155.4	381.4*	181.4	271.9
	180.8	334.15*	206.8	277.75
	206.4	389.05*	225.8	281.45
	225.3	393.5*	244.9	285.5
	244.3	396.7*	263.9	290.0
	263.4	400.05*		
SG Data	66.8	242,395	67.2	278,293
	92.2	275,378	92.6	268
	117.7	342,370	111.4	254
	136.9	367	130.7	260
	155.7	-	149.5	267
Predetonation vel., mm/ μs	0.08 - 0.44		0.29	
λ (mm)	134(130 ⁺⁵)		138	
⁴¹ Δt_D (μs)	228		263	
¹⁵⁶ Δt_D (μs)	-		-	
D(σ) mm/ μs	5.55(0.18)		4.70(0.07)	

*Custom-made probes.

** $\rho_V = 1.88 \text{ g/cm}^3$.

- a. Values in parentheses from IP record.
 b. Conductivity probe.

Units of x and t are mm and μs , respectively.

TABLE A3

DETAILED DATA FOR CUBES AND SLUGS OF VLU-10

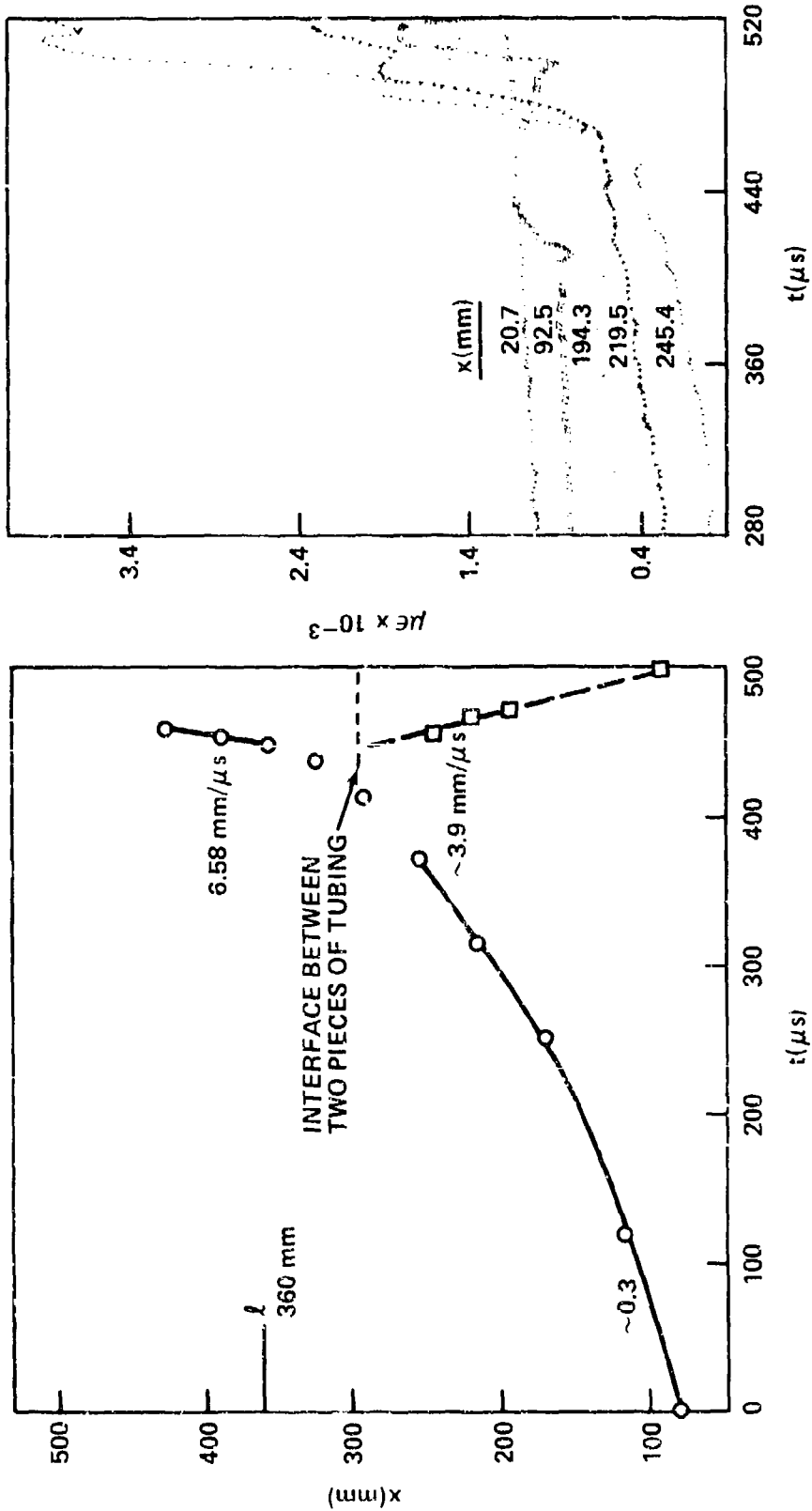
Shot No.	1104		711		808	
Material	Cubes (~1/16 in.)		Cubes (~1/8 in.)		Slugs 0.64 in. dia. x 2 in. long	
Density $\rho_0, \text{g/cm}^3$	1.12		1.10			
%TMD**	59.6		58.5		~95	
IP Data	<u>x</u>	<u>t</u>	<u>x</u>	<u>t</u>	<u>x</u>	<u>t</u>
	41.7	- ^a	There were responses		41.4	-*
	60.7	-*	from only two or		54.1	0.0*
	79.9	0.0*	three IPs on this		79.5	93.9*
	105.3	-*	shot. They could		104.9	192.15*
	130.8	30.65*	not be identified,		130.3	336.9*
	149.7	56.8*	but one triggered		155.7	348.9*
	168.8	100.6*	the scopes for the		181.1	357.3*
	187.8	128.75*	SG records.		206.5	378.2*
	206.9	137.0*			231.9	399.8*
	226.1	143.3*			257.3	440.1*
	245.0	148.0*				
	264.2	151.85*				
SG Data	20.3	-, 169, 185	20.6	180, 274, 313	20.3	502
	66.8	52-64, 161, 180	54.	-	41.1	385, 570
	105.0	66, -, 154	79.9	168, 241, 323, 350-65	67.1	360, 595
	143.0	93, -, 144	105.2	180, 330, 357	136.7	326
	181.1	113, -, -	130.7	180, 335, 342-353	187.7	316
Predetonation vel., mm/ μs	-		This shot failed to transit. The tube was nearly intact (far end closure blown off and end of tube slightly expanded). All propellant burned.		0.27 - 2.5 - 0.63 No detonation. Despite decreasing velocity of IP front, pressure continued to rise. Tube split into two pieces at ca. 850 μs .	
x (mm)	232(230-0)	+5				
$41 \Delta t_D$ (μs)	-					
$156 \Delta t_D$ (μs)	73.5					
$D(\sigma)$ mm/ μs	5.0(-)					

* Custom-made probes.

** $\rho_v = 1.88 \text{ g/cm}^3$.

a. Conductivity probes.

Units of x and t are mm and μs , respectively.



a. DISTANCE-TIME DATA. (O CUSTOM-MADE PROBE, ● COMMERCIAL PROBE, ◐ CONDUCTIVITY PROBE, X LOCATION OF C-M PROBE SHOWING NO RESPONSE, Δ PARTIAL DISCHARGE OF IP, ◊ PROBE LOCATION DUBIOUS.)

b. STRAIN-TIME DATA. (EACH CURVE, EXCEPT THE LOWEST, HAS BEEN RAISED $200 \mu\epsilon$ -OR AN INTEGRAL MULTIPLE THEREOF -FOR BETTER DATA DISPLAY.)

FIGURE A1 SHOT 1001 ON 90.5% TMD sVLU-10, $\rho_0 = 1.70 \text{ g/cm}^3$

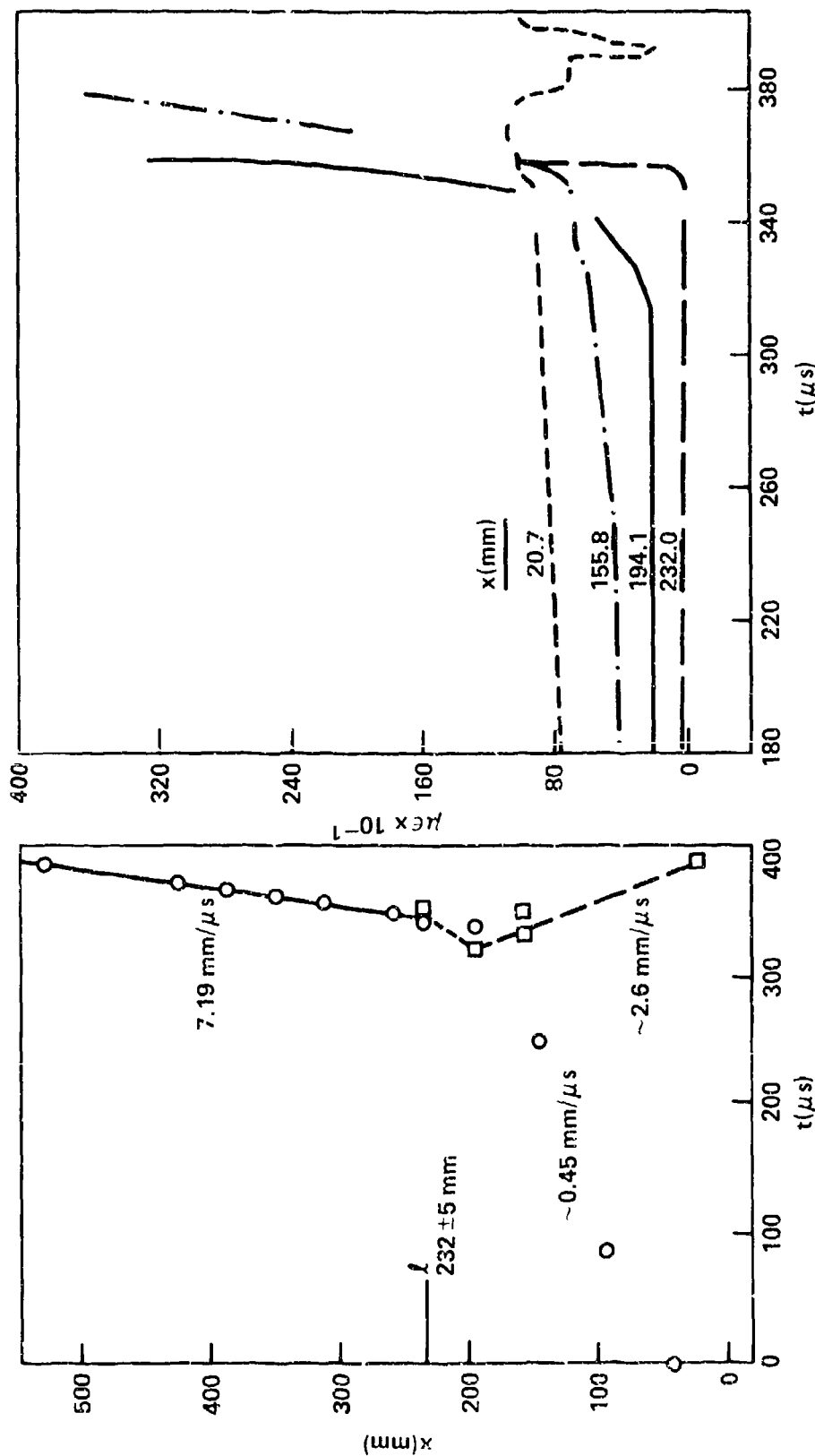


FIGURE A2 SHOT 902 ON 86.6% TMD sVLU-10, $\rho_0 = 1.63 \text{ g/cm}^3$ (KEYS OF FIGURE A1)

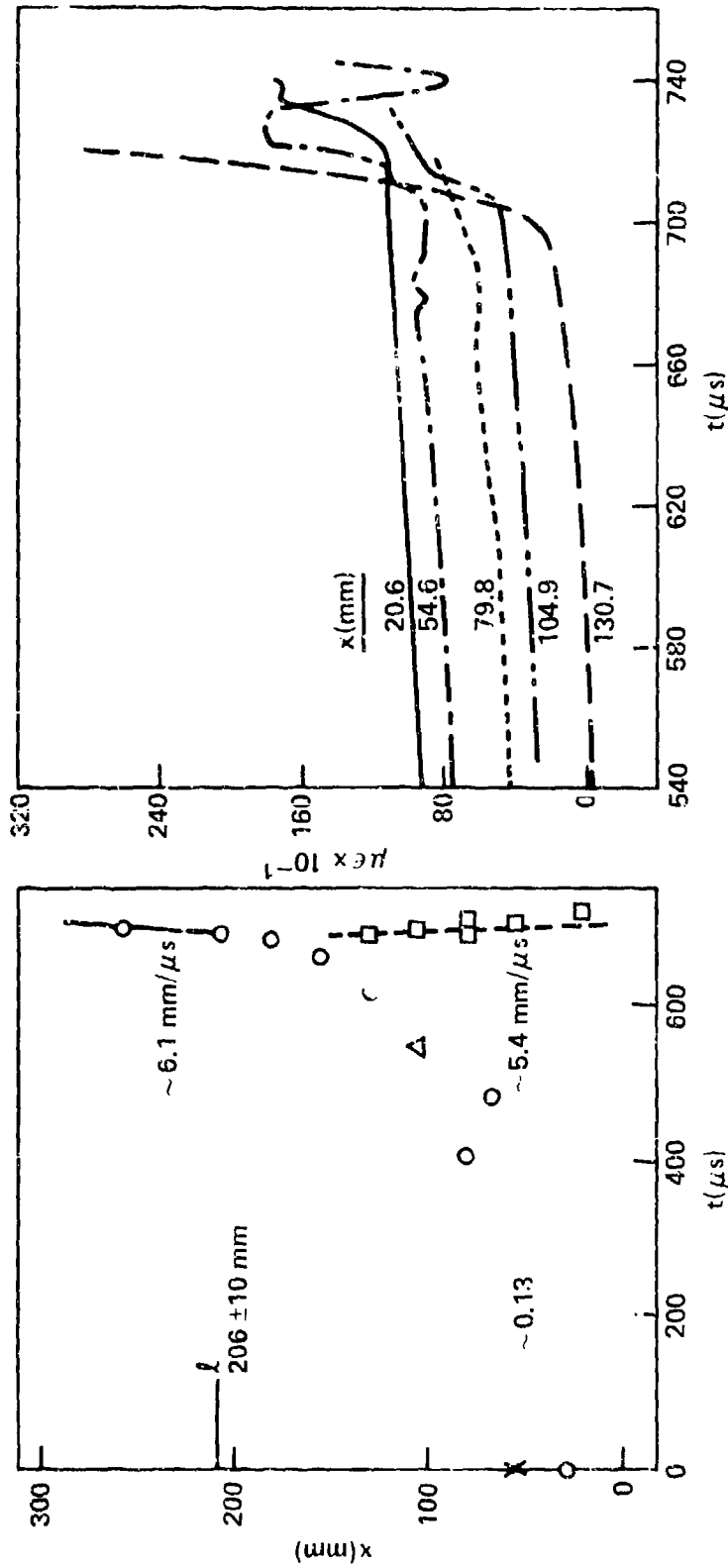


FIGURE A3 SHOT 802 ON 82.6% TMD sVLU-10, $\rho_0 = 1.55 \text{ g/cm}^3$ (KEYS OF FIGURE A1)

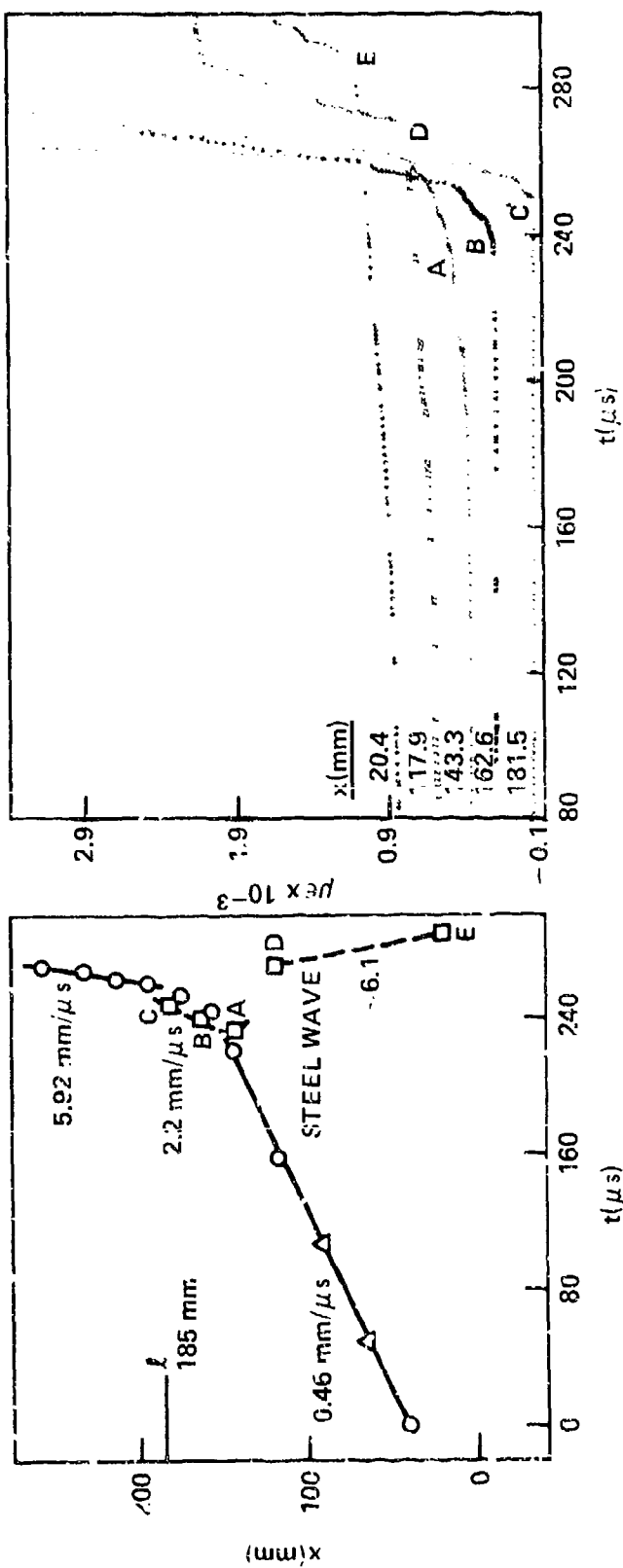
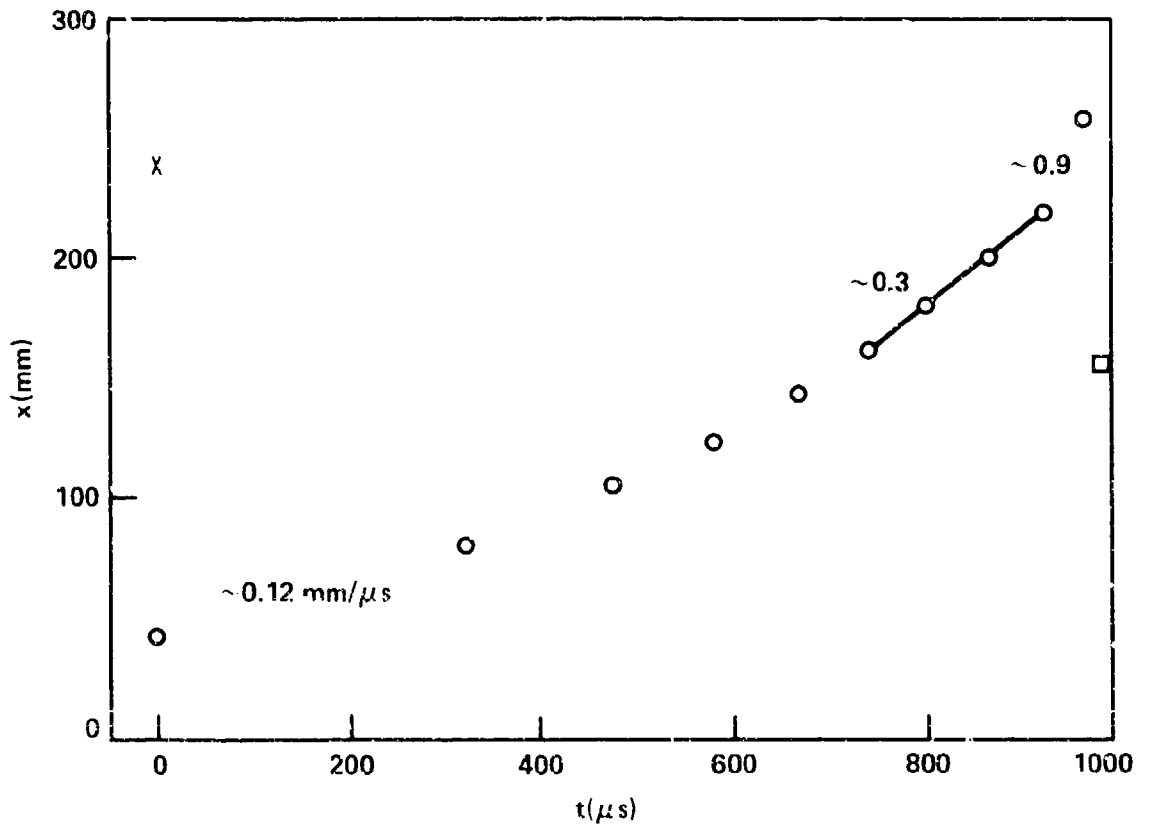
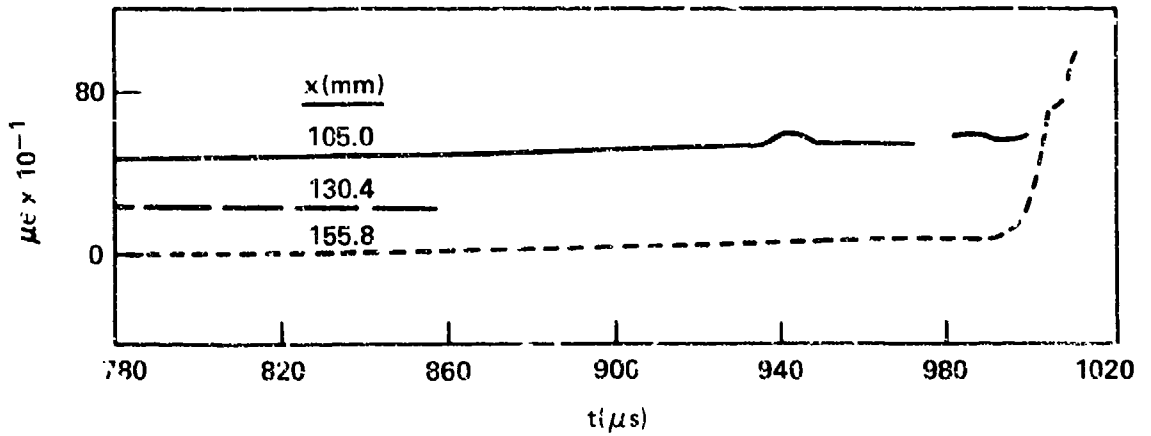


FIGURE A4 SHOT 803 ON 78.7% TMD sVLU-10, $\rho_0 = 1.48 \text{ g/cm}^3$ (KEYS OF FIGURE A1)

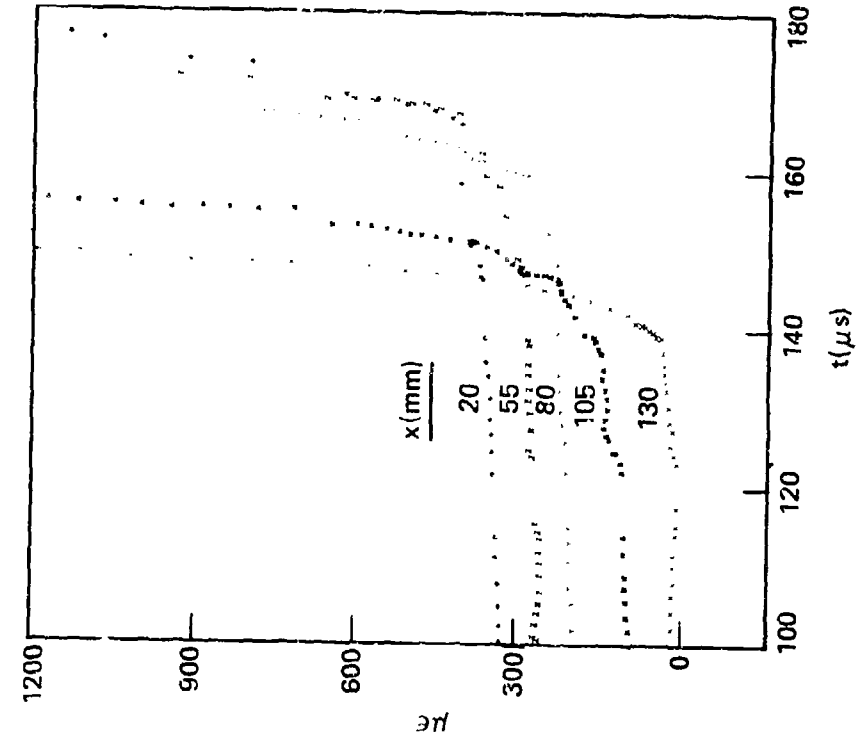


a. DISTANCE-TIME DATA

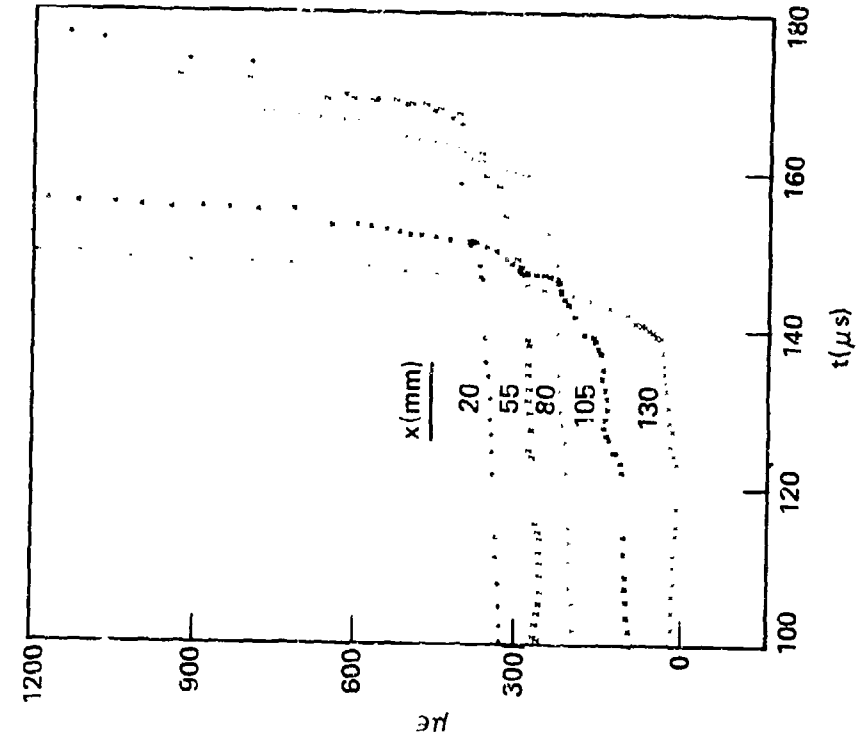


b. STRAIN-TIME DATA

FIGURE A5 SH 817 ON 74.5% TMD sVLU-10, $\rho_0 = 1.40 \text{ g/cm}^3$ (KEYS OF FIGURE A1)

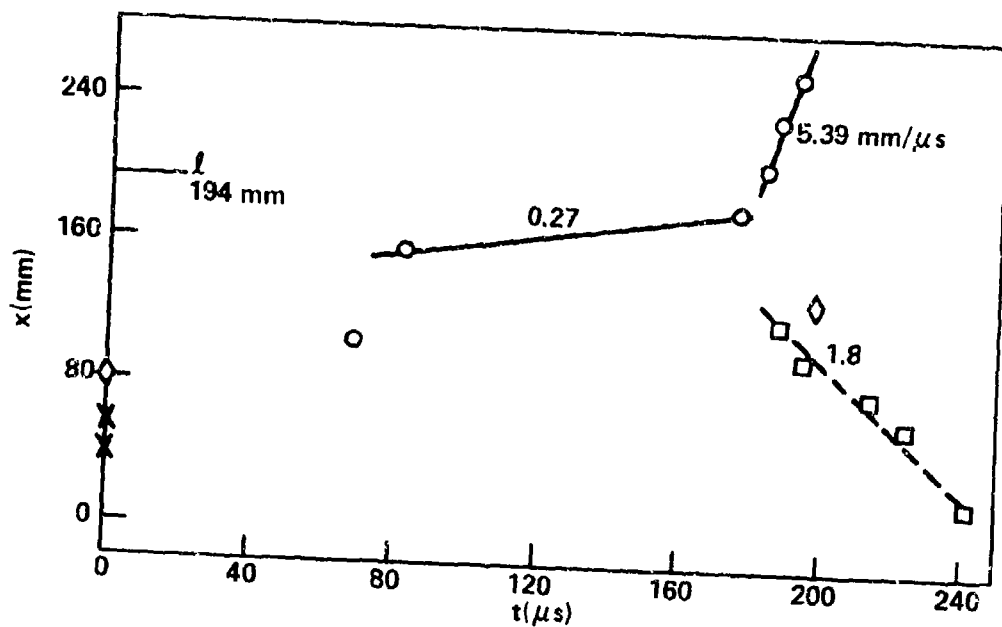


a. DISTANCE-TIME DATA

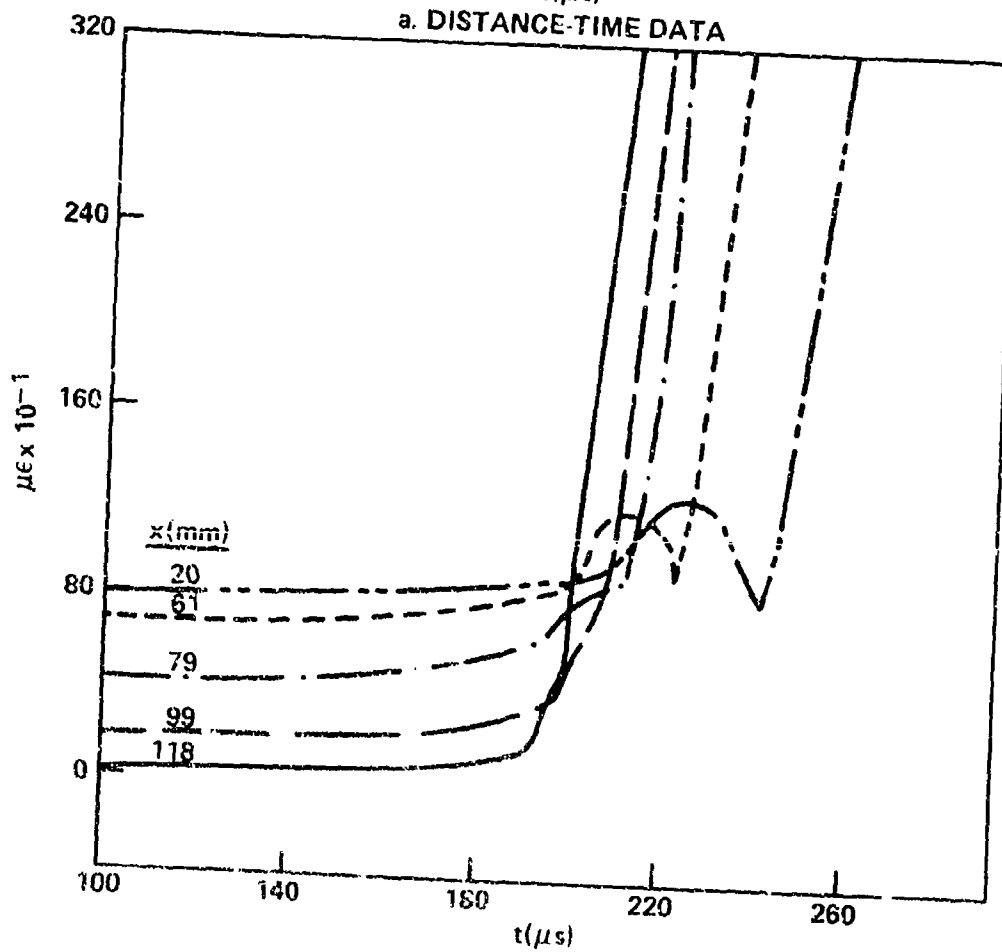


b. STRAIN-TIME DATA (75 $\mu\epsilon$ INTERVAL)

FIGURE A6 SHOT 712 ON 74.5% TMD sVLJ-10, $\rho_0 = 1.40 \text{ g/cm}^3$ (KEYS OF FIGURE A1)



a. DISTANCE-TIME DATA



b. STRAIN-TIME DATA

FIGURE A7 SHOT 710 ON 64.4% TMD s/1U-10, $\rho_0=1.21$ g/cm³ (KEYS OF FIGURE A1)

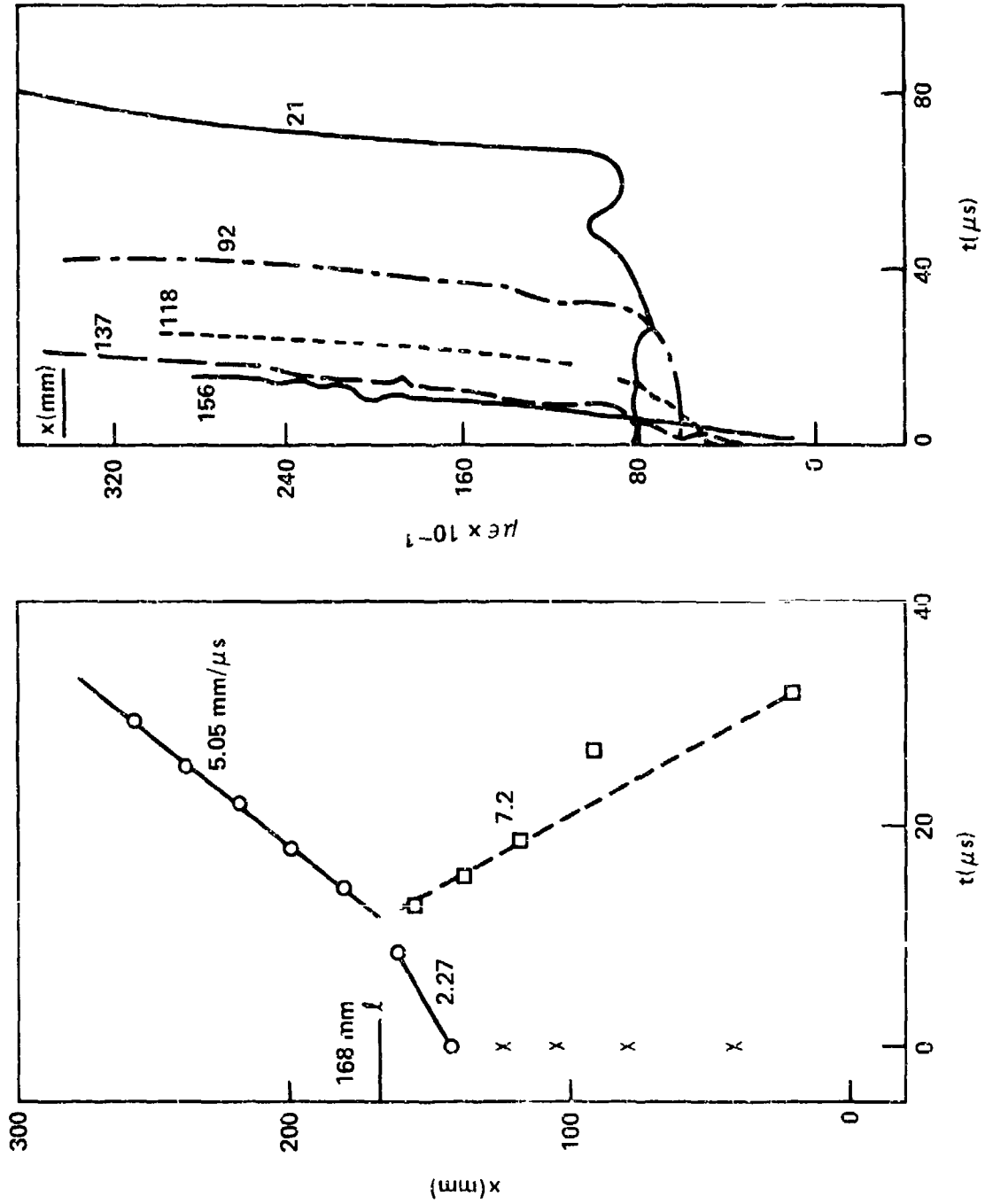
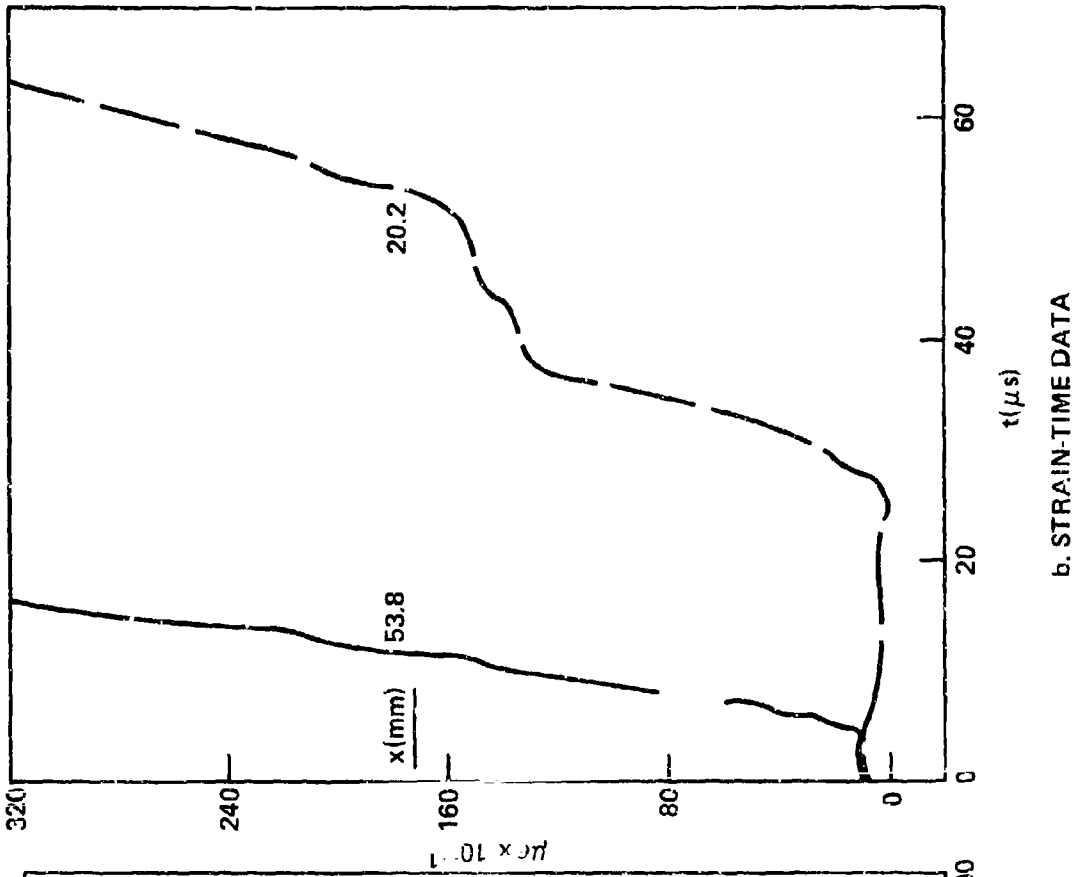
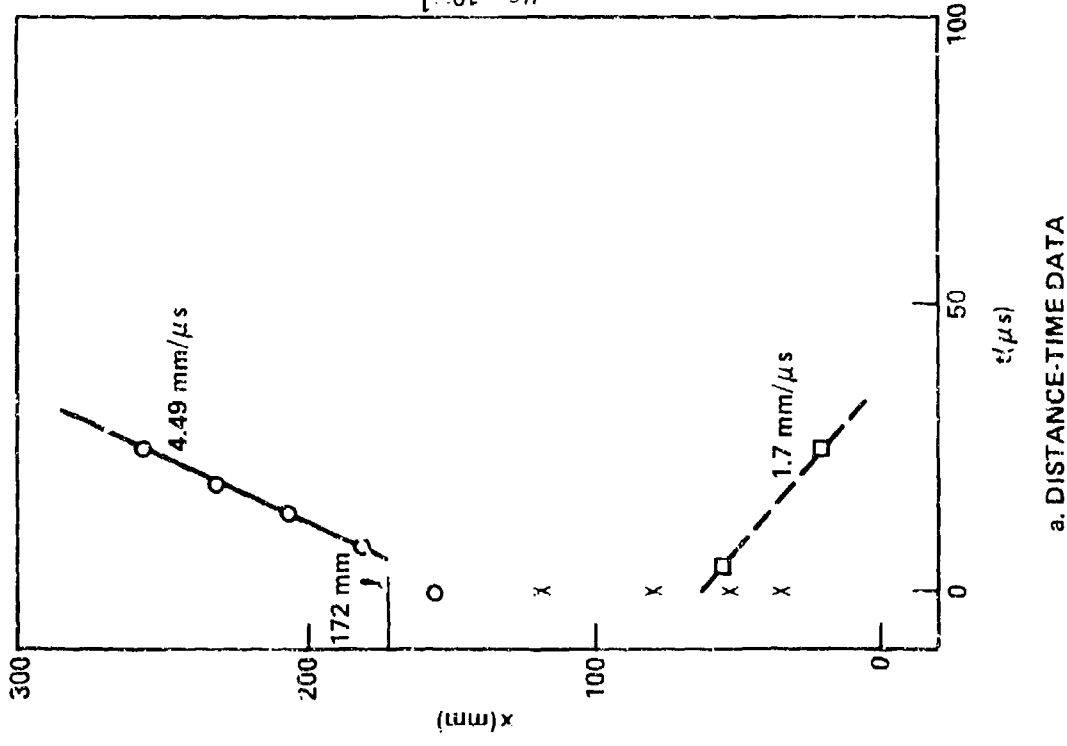


FIGURE A8 SHOT 901 ON 60.4% TMD sVLU-10, $\rho_0 = 1.14 \text{ g/cm}^3$ (KEYS OF FIGURE A1)

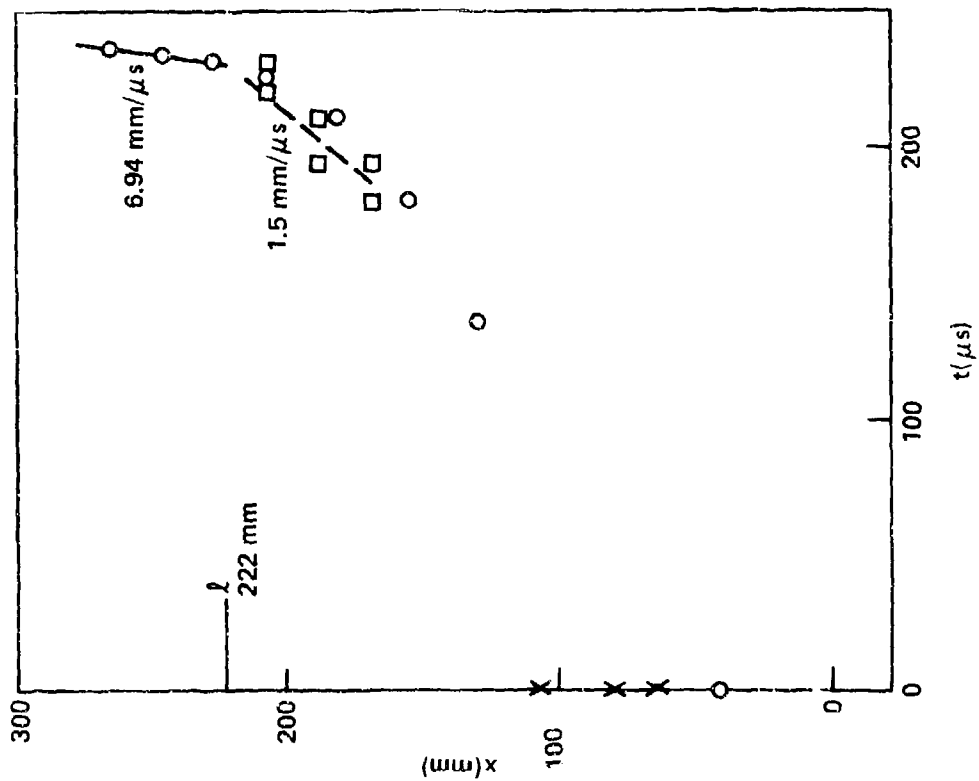


b. STRAIN-TIME DATA

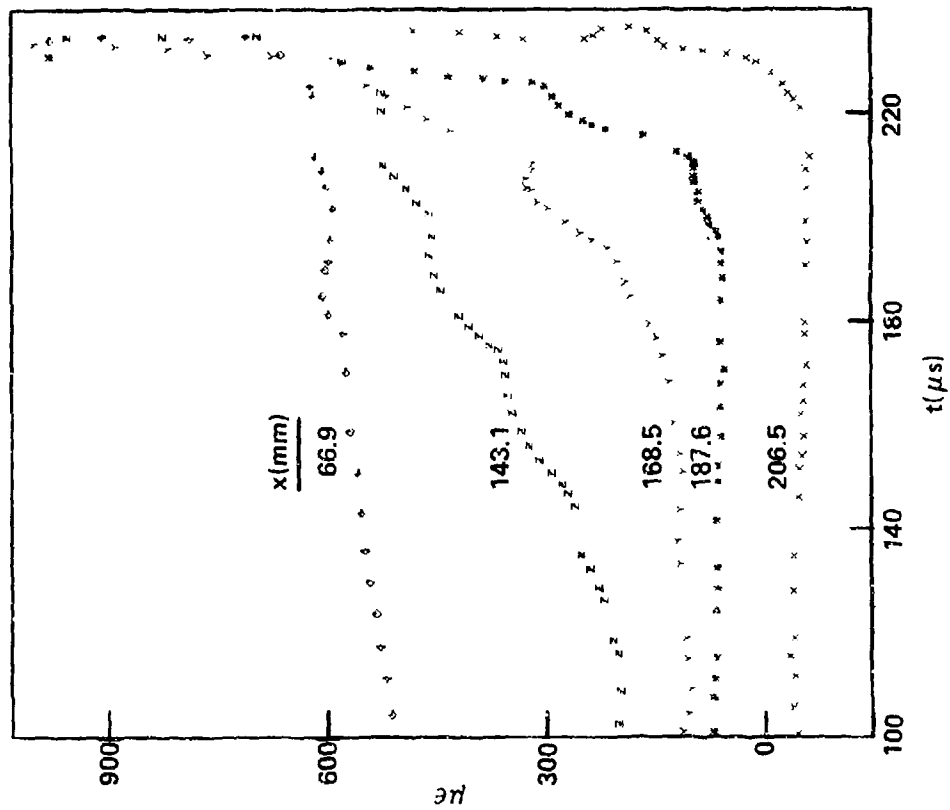


a. DISTANCE-TIME DATA

FIGURE A9 SHOT 709 ON 54.3% TMD sVLU-10, $\rho_0 = 1.02 \text{ g/cm}^3$ (KEYS OF FIGURE A1)



a. DISTANCE-TIME DATA

b. STRAIN-TIME DATA (75 $\mu\epsilon$ INTERNAL)FIGURE A10 SHOT 1219 ON 86.2% TMD pVLJ-10, $\rho_0 = 1.62 \text{ g/cm}^3$ (KEYS OF FIGURE A1)

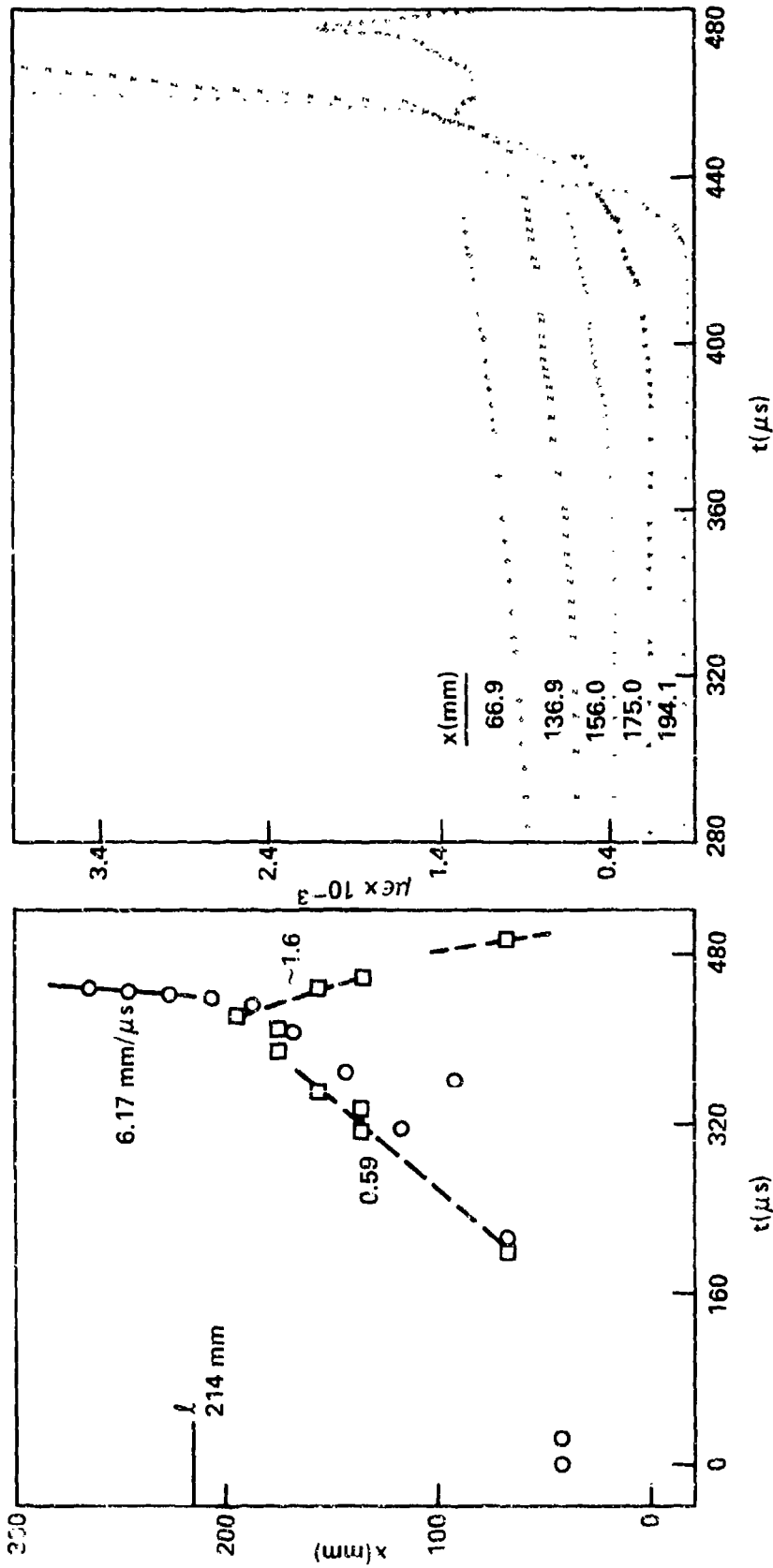
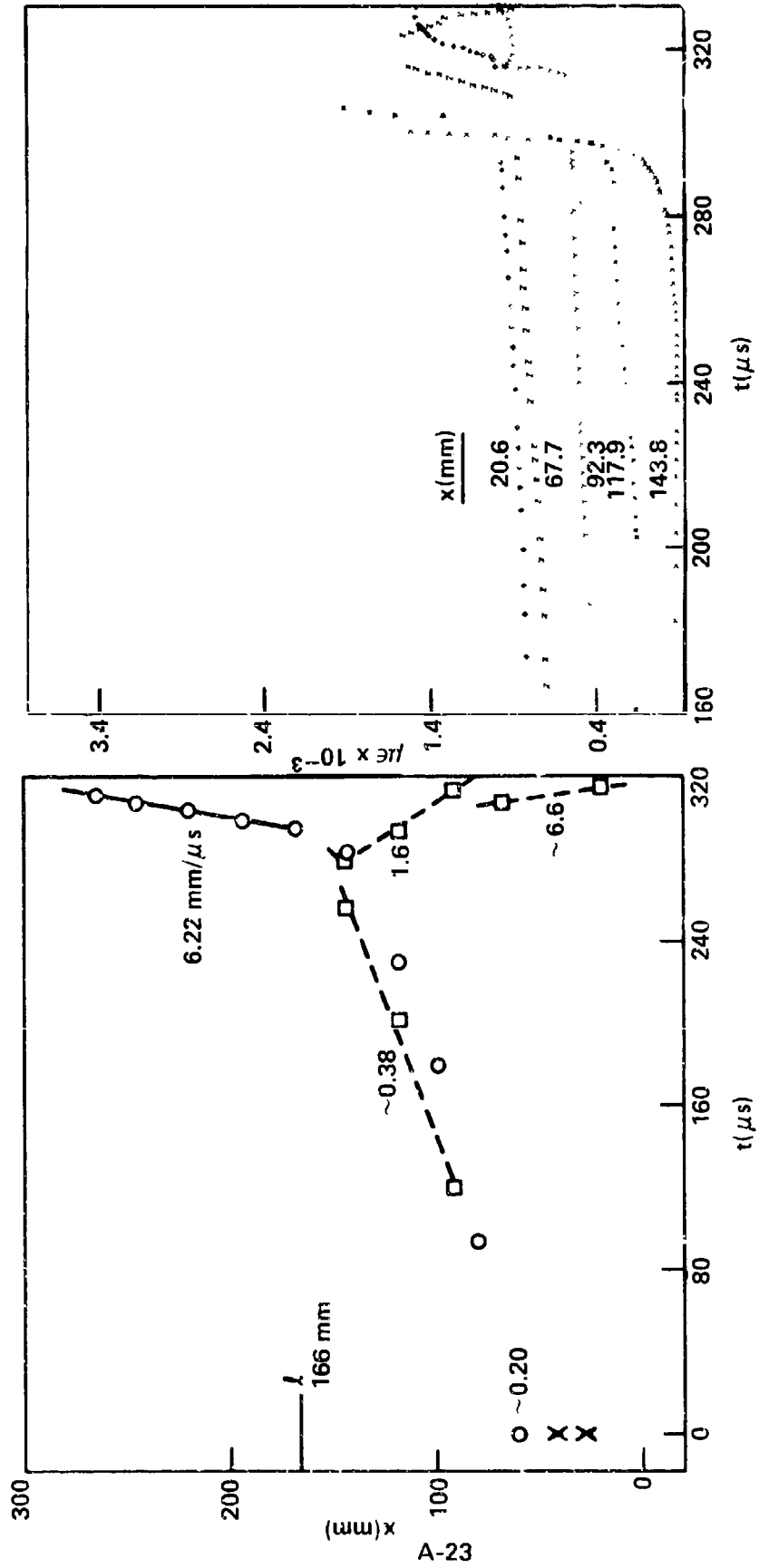


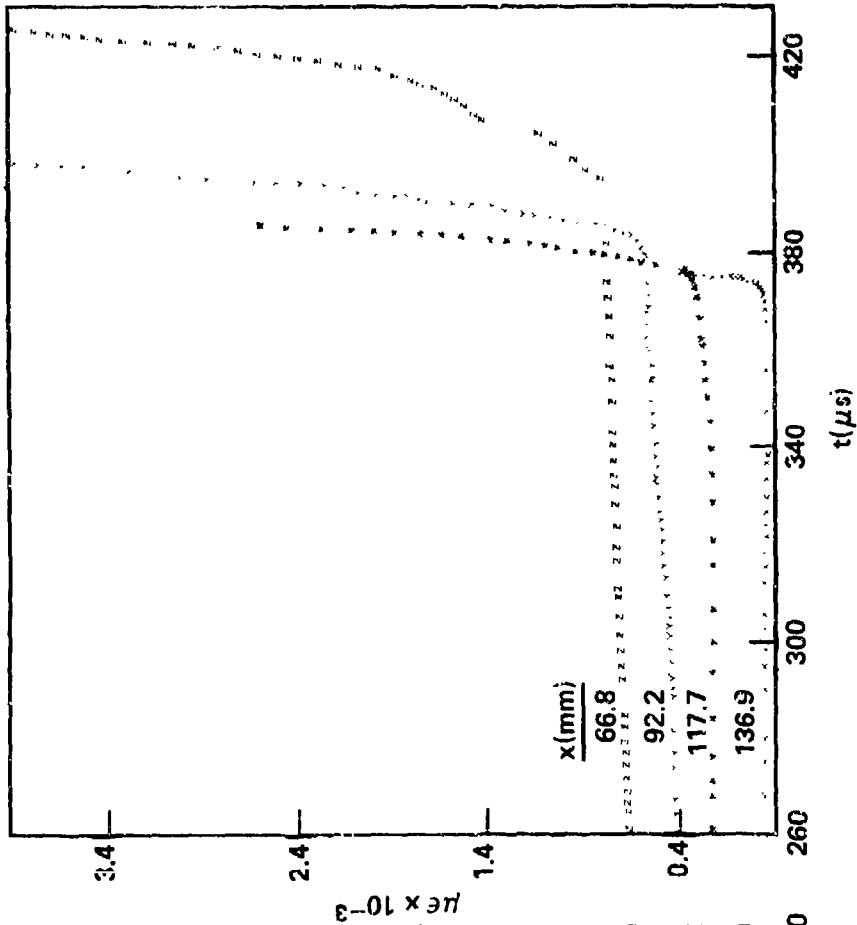
FIGURE A11 SHOT 1201 ON 83.8% TMD pVLU-10, $\rho_0 = 1.58 \text{ g/cm}^3$ (KEYS OF FIGURE A1)



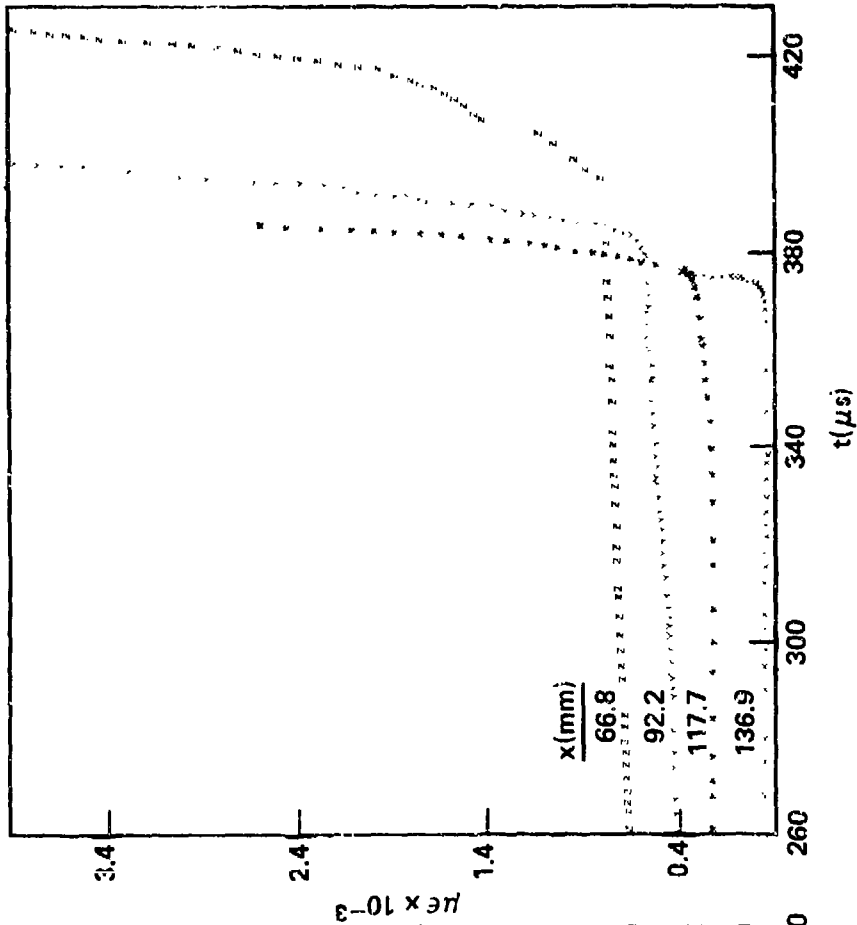
b. STRAIN-TIME DATA

a. DISTANCE-TIME DATA

FIGURE A12 SHOT 1016 ON 74.6% TMD pVLU-10, $\rho_0 = 1.40 \text{ g/cm}^3$ (KEYS OF FIGURE A1)

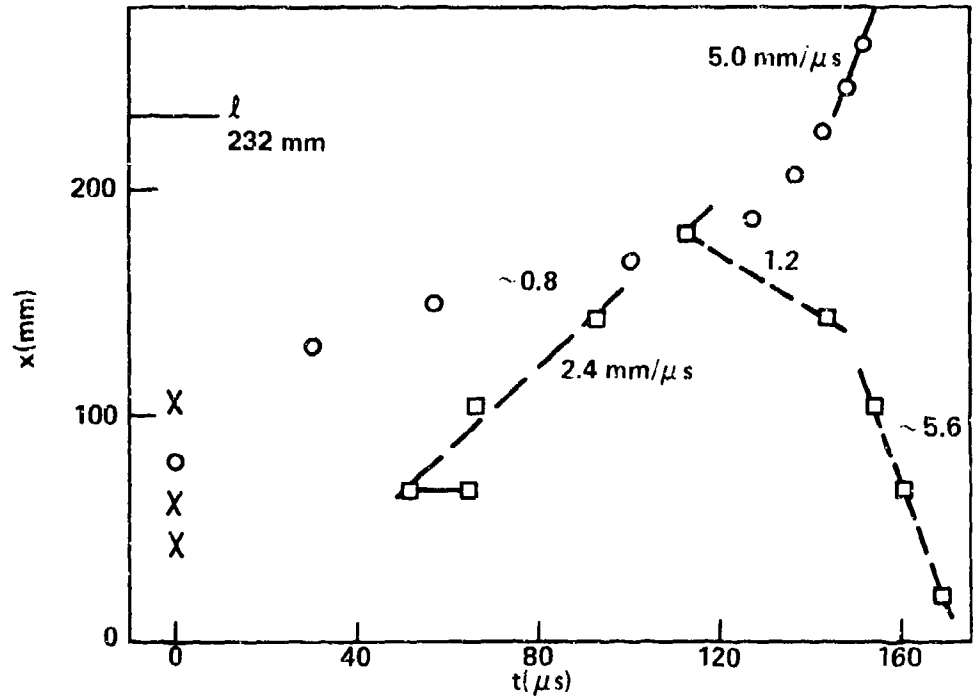


a. DISTANCE-TIME DATA

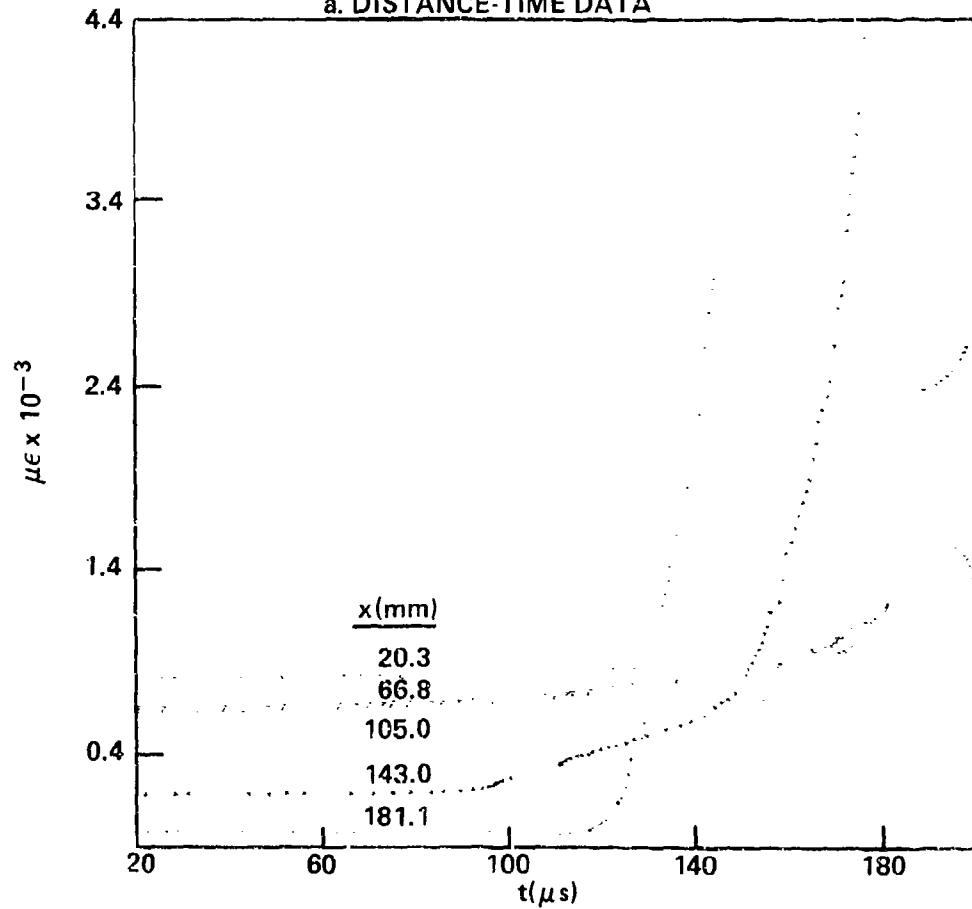


b. STRAIN-TIME DATA

FIGURE A13 SHOT 1211 ON 65.4% TMD pVLU-10, $\rho_0 = 1.23 \text{ g/cm}^3$ (KEYS OF FIGURE A1)

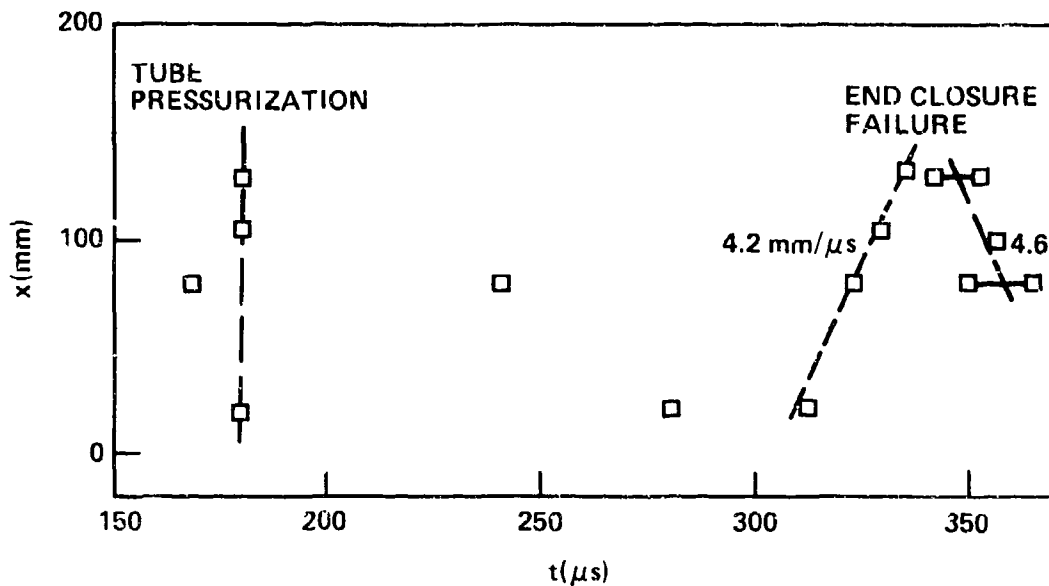


a. DISTANCE-TIME DATA

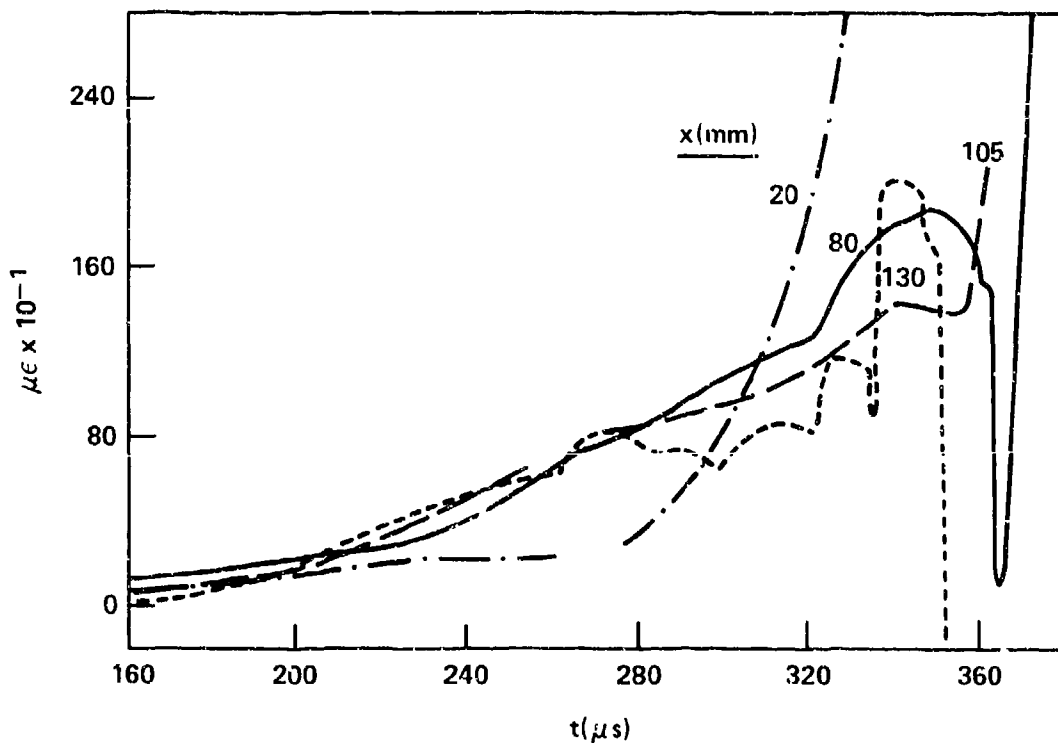


b. STRAIN-TIME DATA

FIGURE A14 SHOT 1104 ON 59.6% TMD CUBED VLU-10, $\rho_0 = 1.12 \text{ g/cm}^3$ (KEYS OF FIGURE A1)

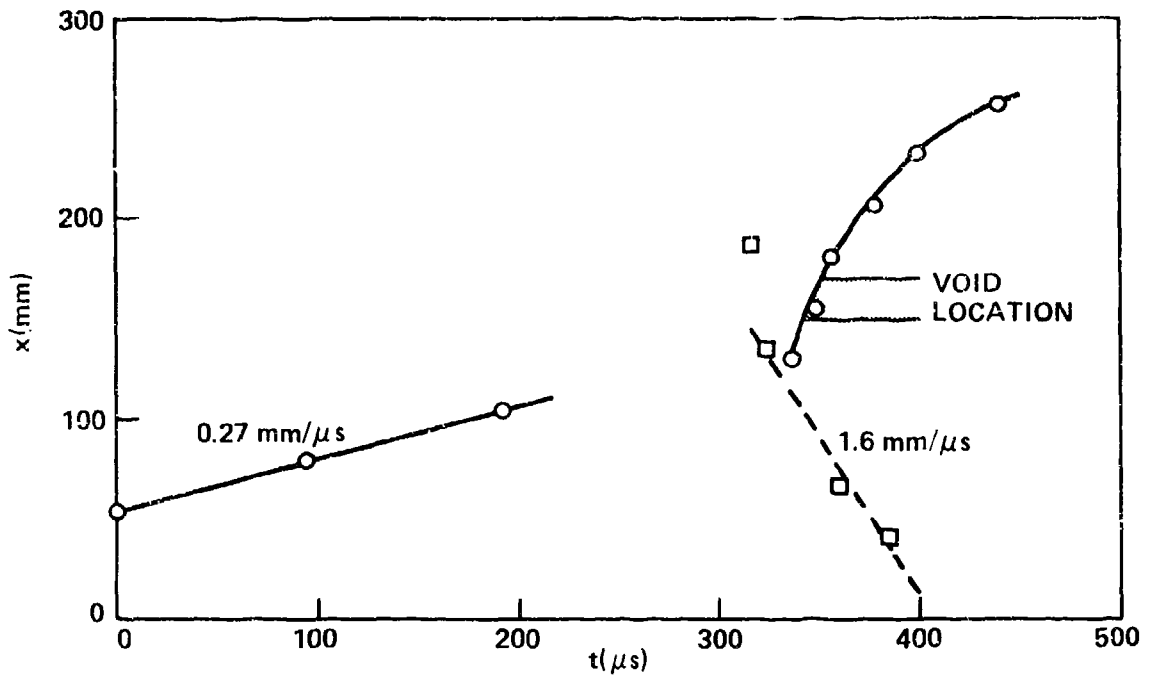


a. DISTANCE-TIME DATA

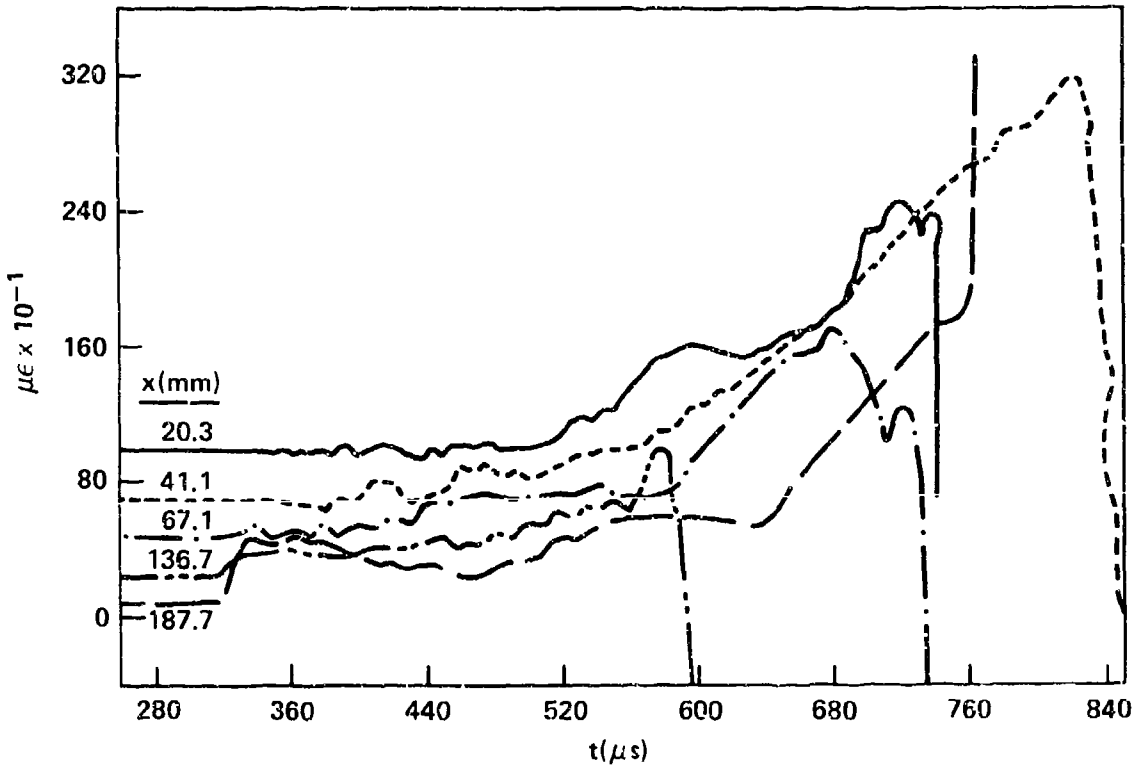


b. STRAIN-TIME DATA (ZERO $\mu\epsilon$ INTERVAL)

FIGURE A15 SHOT 711 ON 58.5% TMD CUBED VLU-10, $\rho_0 = 1.10 \text{ g/cm}^3$ (KEYS OF FIGURE A1)



a. DISTANCE-TIME DATA



b. STRAIN-TIME DATA

FIGURE A16 SHOT 808 ON ~100% TMD SLUGS OF VLU-10, $\rho_0 \sim 1.88 \text{ g}/\text{cm}^3$ (KEYS OF FIGURE A1)

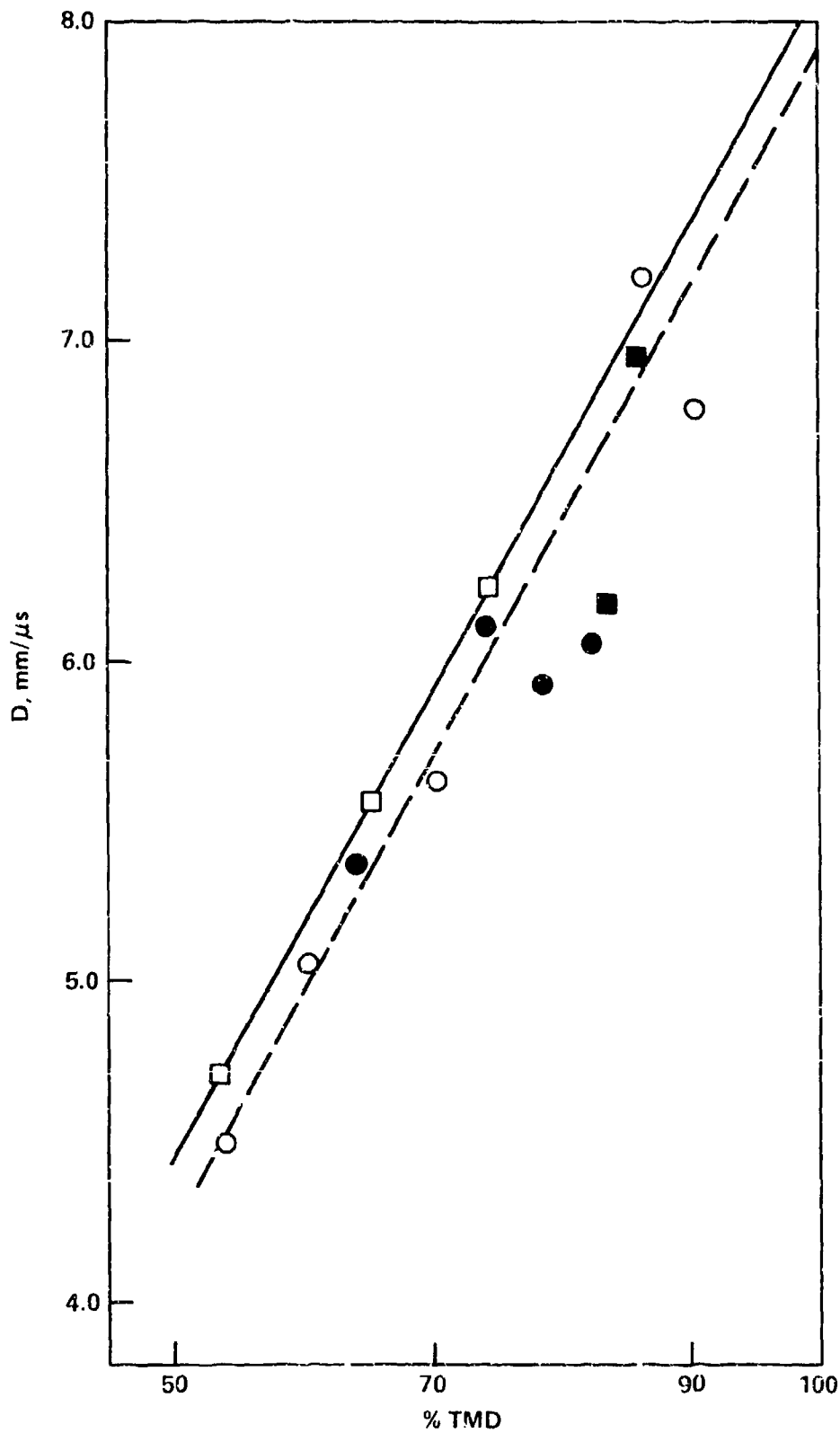


FIGURE A17 DETONATION VELOCITY OF VLU-10 AS A FUNCTION OF % TMD)

(○ sVLU, $\sigma \leq 0.2$; □ pVLU, $\sigma \leq 0.2$
 ● sVLU, $\sigma > 0.2$; ■ pVLU, $\sigma > 0.2$)

DISTRIBUTION

Chief of Naval Material
Washington, DC 20360

Commander
Naval Air Systems Command
Attn: AIR-350
AIR-330
Department of the Navy
Washington, DC 20361

Commander
Naval Sea Systems Command
Attn: Technical Library
SEA-03B
SEA-62R
SEA-62R2
SEA-62R3
SEA-62R32
SEA-64E
Department of the Navy
Washington, DC 20360

Director
Strategic Systems Project Office (PM-1)
Attn: SP-273 (R. M. Kinert)
SP-27311 (E. L. Throckmorton, Jr.)
Department of the Navy
Washington, DC 20376

Office of Naval Research
Attn: Rear Admiral C. O. Holmquist
ONR-741 (Technical Library)
Department of the Navy
Arlington, VA 22217

2

DISTRIBUTION (Cont.)

Commander
Naval Weapons Center
Attn: Code 556
 Technical Library
 H. D. Mallory
 Code 452
 Code 5008
 R. L. Derr 2
China Lake, CA 93555

Director
Naval Research Laboratory
Attn: Technical Information Section 2
Washington, DC 20375

Office of Chief of Naval Operations
Operations Evaluation Group (OP03EG)
Washington, DC 20350

Director
Office of the Secretary of Defense
Advanced Research Projects Agency
Washington, DC 20301

Commanding Officer
Naval Weapons Station
Attn: R&D Division
 Code 50
Yorktown, VA 23691

Commanding Officer
Naval Propellant Plant
Attn: Technical Library
Indian Head, MD 20640

Commanding Officer
Naval Explosive Ordnance Disposal Facility
Attn: Information Services
Indian Head, MD 20640

McDonnell Aircraft Company
Attn: M. L. Schimmel
P. O. Box 516
St. Louis, MO 63166

DISTRIBUTION (Cont.)

Commanding Officer
Naval Ammunition Depot
Crane, IN 47522

Commanding Officer
Naval Underwater Systems Center
Attn: LA 151-Technical Library
Newport, RI 02840

Commanding Officer
Naval Weapons Evaluation Facility
Attn: Code AT-7
Kirtland Air Force Base
Albuquerque, NM 87117

Commanding Officer
Naval Ammunition Depot
Attn: QEL
Concord, CA 94522

Superintendent Naval Academy
Attn: Library
Annapolis, MD 21402

Naval Plant Representative Office
Strategic Systems Project Office
Lockheed Missiles and Space Company
Attn: SPL-332 (R. H. Guay)
P. O. Box 504
Sunnyvale, CA 94088

Hercules Incorporated
Allegany Ballistics Laboratory
Attn: Library
P. O. Box 210
Cumberland, MD 21502

AMCRD
5001 Eisenhower Avenue
Alexandria, VA 22302

Redstone Scientific Information Center
U. S. Army Missile Command
Attn: Chief, Documents
Redstone Arsenal, AL 35809

DISTRIBUTION (Cont.)

Commanding Officer
Army Armament Research and
Development Command
Energetic Materials Division
Attn: Louis Aurami, DRDAR-LCE
Dover, NJ 07801

Commanding General
Attn: BRL
Aberdeen Proving Ground, MD 21005

Commanding Officer
Harry Diamond Laboratories
Attn: Library
2800 Powder Mill Road
Adelphi, MD 20783

Armament Development & Test Center
DLDSL/Technical Library
Eglin Air Force Base, Florida 32542

Commanding Officer
Naval Ordnance Station
Louisville, KY 40124

Director
Applied Physics Laboratory
Attn: Library
Johns Hopkins Road
Laurel, MD 20810

U. S. Department of Energy
Attn: DMA
Washington, DC 20545

Director
Defense Nuclear Agency
Washington, DC 20305

2

Research Director
Pittsburgh Mining and Safety
Research Center
Bureau of Mines
Attn: R. W. Var Dolah
4800 Forbes Avenue
Pittsburgh, PA 15213

DISTRIBUTION (Cont.)

Director
Defense Documentation Center
Cameron Station
Alexandria, VA 22314

12

Goddard Space Flight Center, NASA
Glenn Dale Road
Greenbelt, MD 20771

Lawrence Livermore Laboratory
University of California
Attn: M. Finger
 E. James
 F. Lee
 P. Urtiew
P. O. Box 808
Livermore, CA 94551

Sandia Laboratories
Attn: R. J. Lawrence, Div. 5165
P. O. Box 5800
Albuquerque, NM 87115

Director
Los Alamos Scientific Laboratory
Attn: Library
 L. C. Smith
 B. G. Craig
 H. Flaugh
P. O. Box 1663
Los Alamos, NM 87544

DDESB
Forrestal Building, Room GS 270
Washington, DC 20314

Aerojet Ordnance and Manufacturing
Company
9236 East Hall Road
Downey, CA 90241

Hercules Incorporated Research Center
Attn: Technical Information Division
 B. E. Clouser
Wilmington, DE 19899

DISTRIBUTION (Cont.)

Thiokol/Huntsville Division
Attn: Technical Library
Huntsville, AL 35807

Shock Hydrodynamics Division
Whittaker Corporation
Attn: Dr. L. Zernow
4716 Vineland Avenue
North Hollywood, CA 91602

2

Stanford Research Institute
Attn: D. Curran
C. M. Tarver
333 Ravenswood Avenue
Menlo Park, CA 94025

Thiokol/Wasatch Division
Attn: Technical Library
P. O. Box 524
Brigham City, UT 84302

Thiokol/Elkton Division
Attn: Technical Library
P. O. Box 241
Elkton, MD 21921

Teledyne McCormick Selph
P. O. Box 6
Hollister, CA 95023

Lockheed Missiles and Space Division
1122 Jagels Road
Sunnyvale, CA 94086

R. Stresau Laboratory, Inc.
Star Route
Spooner, WI 54801

Rohm and Haas
Huntsville, Defense Contract Office
Attn: H. M. Shuey
723-A Arcadia Circle
Huntsville, AL 35801

DISTRIBUTION (Cont.)

U. S. Army Foreign Service
and Technology Center
220 7th Street, N.E.
Charlottesville, VA 22901

Princeton Combustion Research Laboratories, Inc.
1041 U. S. Highway One North
Attn: M. Summerfield
N. Messina
Princeton, NJ 08540

Pennsylvania State University
Department of Mechanical Engineering
Attn: K. Kuo
University Park, PA 16802

Ballistic Research Laboratories
Attn: N. Gerri
Aberdeen Proving Ground, MD 21005

Paul Gough Associates
1048 South Street
Portsmouth, NH 03801

Hercules Incorporated, Bacchus Works
Attn: B. Hopkins
P. O. Box 98
Magna, UT 84044

Professor H. Krier
A & A Engineering Department
101 Transportation Building
University of Illinois
Urbana, IL 61801

Chemical Propulsion Information Agency
The Johns Hopkins University
Applied Physics Laboratory
Johns Hopkins Road
Laurel, MD 20810

ITT Research Institute
Attn: H. S. Napadensky
10 West 35th Street
Chicago, IL 60616

DISTRIBUTION (Cont.)

Erion Associates, Inc.
Attn: W. Petray
600 New Hampshire Avenue,
Suite 870
Washington, DC 20037

Brigham Young University
Department of Chemical Engineering
Attn: Dr. M. W. Beckstead
Provo, UT 84601

Library of Congress
Attn: Gift and Exchange Division
Washington, DC 20540

4

TO AID IN UPDATING THE DISTRIBUTION LIST
FOR NAVAL SURFACE WEAPONS CENTER, WHITE
OAK TECHNICAL REPORTS PLEASE COMPLETE THE
FORM BELOW:

TO ALL HOLDERS OF NSWC/TR 79-351
by R. R. Bernecker, Code R10

DO NOT RETURN THIS FORM IF ALL INFORMATION IS CURRENT

A. FACILITY NAME AND ADDRESS (OLD) (Show Zip Code)

NEW ADDRESS (Show Zip Code)

B. ATTENTION LINE ADDRESSES:

C.

REMOVE THIS FACILITY FROM THE DISTRIBUTION LIST FOR TECHNICAL REPORTS ON THIS SUBJECT.

D.

NUMBER OF COPIES DESIRED _____

DEPARTMENT OF THE NAVY
NAVAL SURFACE WEAPONS CENTER
WHITE OAK, SILVER SPRING, MD. 20910

OFFICIAL BUSINESS
PENALTY FOR PRIVATE USE, \$300

POSTAGE AND FEES PAID
DEPARTMENT OF THE NAVY
DOD 316



COMMANDER
NAVAL SURFACE WEAPONS CENTER
WHITE OAK, SILVER SPRING, MARYLAND 20910

ATTENTION: CODE R10